
Collapsing Taylor Mode Automatic Differentiation

Felix Dangel*
 Vector Institute
 Toronto, Canada
 fdangel@vectorinstitute.ai

Tim Siebert*
 Humboldt-Universität zu Berlin and
 Zuse Institute Berlin
 Berlin, Germany
 tim.siebert@hu-berlin.de

Marius Zeinhofer
 ETH Zurich
 Zurich, Switzerland,
 marius.zeinhofer@sam.math.ethz.ch

Andrea Walther
 Humboldt-Universität zu Berlin and
 Zuse Institute Berlin
 Berlin, Germany
 andrea.walther@math.hu-berlin.de

Abstract

Computing partial differential equation (PDE) operators via nested backpropagation is expensive, yet popular, and severely restricts their utility for scientific machine learning. Recent advances, like the forward Laplacian and randomizing Taylor mode automatic differentiation (AD), propose forward schemes to address this. We introduce an optimization technique for Taylor mode that “collapses” derivatives by rewriting the computational graph, and demonstrate how to apply it to general linear PDE operators, and randomized Taylor mode. The modifications simply require propagating a sum up the computational graph, which could—or should—be done by a machine learning compiler, without exposing complexity to users. We implement our collapsing procedure and evaluate it on popular PDE operators, confirming it accelerates Taylor mode and outperforms nested backpropagation.

1 Introduction

Using neural networks to learn functions constrained by physical laws is a popular trend in scientific machine learning [4, 16–18, 23, 24, 28]. Typically, the Physics is encoded through partial differential equations (PDEs) that the neural net must satisfy. The associated loss functions require evaluating differential operators w.r.t. the net’s input, rather than weights. Evaluating these differential operators remains a computational challenge, especially if they contain high-order derivatives.

Computing PDE operators. Two important fields that build on PDE operators are variational Monte-Carlo (VMC) simulations and Physics-informed neural networks (PINNs). VMC employs neural networks as ansatz for the Schrödinger equation [4, 16, 23] and demands computing the net’s Laplacian (the Hessian trace) for the Hamiltonian’s kinetic term. PINNs represent PDE solutions as a neural net and train it by minimizing the residuals of the governing equations [18, 24]. For instance, Kolmogorov-type equations like the Fokker-Planck and Black-Scholes equation require weighted second-order derivatives on high-dimensional spatial domains [17, 27]. Other PINNs for elasticity problems use the biharmonic operator [7, 17, 26, 30], which contains fourth-order derivatives.

Is backpropagation all we need? Although nesting first-order automatic differentiation (AD) to compute high-order derivatives scales exponentially w.r.t. the degree in time and memory [26, §3.2],

Preprint.

*Equal contribution

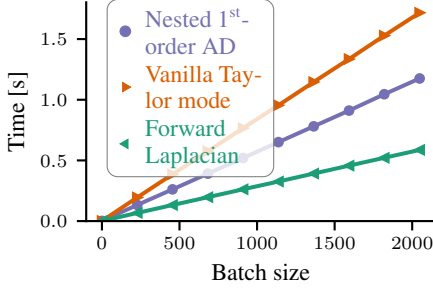
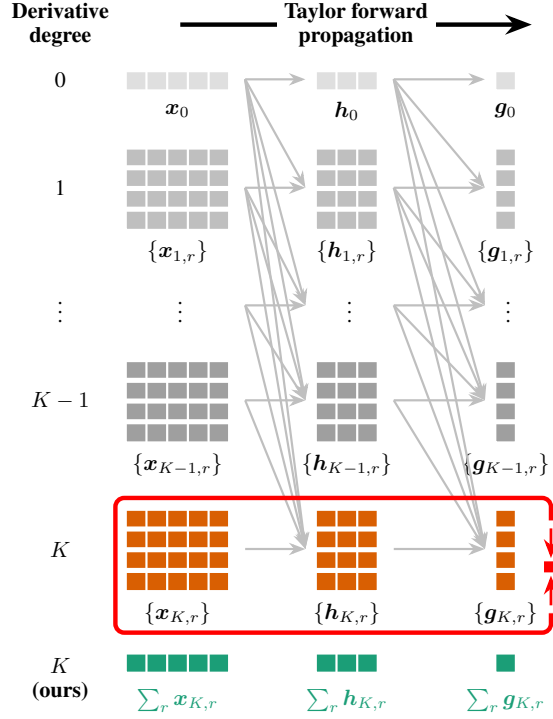


Figure 1: **▲ Vanilla Taylor mode is not enough to beat nested 1st-order AD.** Illustrated for computing the Laplacian of a \tanh -activated $50 \rightarrow 768 \rightarrow 768 \rightarrow 512 \rightarrow 512 \rightarrow 1$ MLP with JAX (+ `jit`) on GPU (details in §G). We show how to automatically obtain the specialized forward Laplacian through simple graph transformations that “collapse” vanilla Taylor mode.

Figure 2: **► Collapsed Taylor mode directly propagates the sum of highest degree coefficients.** Visualized for pushing 4 K -jets through a $\mathbb{R}^5 \rightarrow \mathbb{R}^3 \rightarrow \mathbb{R}$ function ($K = 2$ yields the forward Laplacian).



this approach is common practice: it is easy to implement in ML libraries, and their backpropagation is highly optimized. A promising alternative is *Taylor mode AD* [or simply *Taylor mode*, 13, §13], introduced to the ML community in 2019, which scales polynomially w.r.t. the degree in time and memory [14]. However, we observe empirically that vanilla Taylor mode may not be enough to beat nesting (fig. 1): evaluating the Laplacian of a 5-layer MLP, using JAX’s *Taylor mode* is 50% slower than nested backpropagation that computes, then traces, the Hessian via Hessian-vector products [22]. This calls into question the relevance of Taylor mode for computing common PDE operators.

The advent of forward schemes. Recent works have successfully demonstrated the potential of modified forward propagation schemes, though. For the Laplacian, Li et al. [19, 20] developed a special forward propagation framework called the *forward Laplacian*, whose JAX implementation [12] is roughly twice as fast as nested first-order AD (fig. 1). While the forward Laplacian does not rely on Taylor mode, recent work pointed out a connection [6]; it remains unclear, though, if efficient forward schemes exist for other differential operators, and how they relate to Taylor mode. Concurrently, Shi et al. [26] derived stochastic approximations of differential operators in high dimensions by evaluating Taylor mode along suitably sampled random directions.

Irrespective of stochastic or exact computation, at their core, these popular PDE operators are *linear*: we must evaluate derivatives along multiple directions, then sum them. Based on this linearity, we identify an optimization technique to rewrite the computational graph of standard Taylor mode that is applicable to general linear PDE operators and randomized Taylor mode:

1. **We propose optimizing standard Taylor mode by collapsing the highest Taylor coefficients,** directly **propagating their sum**, rather than **propagating then summing** (fig. 2). Our approach contains the forward Laplacian as special case, is applicable to randomized Taylor mode, and also general linear PDE operators, which we show using the techniques from Griewank et al. [14].
2. **We show how to collapse standard Taylor mode by simple graph rewrites based on linearity.** This leads to a clean separation of concepts: Users can build their computational graph using standard Taylor mode, then rewrite it to collapse it. Due to the simple nature of our proposed rewrites, they could easily be absorbed into the just-in-time (JIT) compilation of ML frameworks without introducing a new interface or exposing complexity to users.

3. **We empirically demonstrate that collapsing Taylor mode accelerates standard Taylor mode.** We implement a Taylor mode library for PyTorch [21] that realizes the graph simplifications with `torch.fx` [25]. On popular PDE operators, we empirically find that, compared to standard Taylor mode, collapsed Taylor mode achieves superior performance that is well-aligned with the theoretical expectation, while consistently outperforming nested first-order AD.

Our work takes an important step towards the broader adoption of Taylor mode as viable alternative to nested first-order AD for computing PDE operators, while being as easy to use.

2 Background: Introduction to Taylor Mode AD

Taylor mode AD (or, simply, Taylor mode) computes higher-order derivatives—as needed, e.g., for PDE operators—through propagation of Taylor coefficients according to the chain rule.

Scalar case. To illustrate Taylor mode, consider the scalar function $f : \mathbb{R} \rightarrow \mathbb{R}$ and extend the input variable x to a path $x(t)$ with $x(0) = x_0$, whose form is a univariate Taylor polynomial of degree K , $x(t) = \sum_{k=0}^K \frac{t^k}{k!} x_k$ with x_k the k -th Taylor coefficient. If f is smooth enough, we can evaluate Taylor coefficients of the transformed path $f(x(t)) = \sum_{k=0}^K \frac{t^k}{k!} f_k$ with $f_k := \frac{d^k}{dt^k} f(x(t))|_{t=0}$. The chain rule provides the coefficients’ propagation rules. E.g., for degree $K = 3$ we get

$$\begin{aligned} f_0 &= f(x_0), & f_2 &= \partial^2 f(x_0) x_1^2 + \partial f(x_0) x_2, \\ f_1 &= \partial f(x_0) x_1, & f_3 &= \partial^3 f(x_0) x_1^3 + 3\partial^2 f(x_0) x_1 x_2 + \partial f(x_0) x_3. \end{aligned} \quad (1)$$

Faà Di Bruno [9] provided the general formula for f_k , and Fraenkel [11] extended it to the multivariate case [see also 1, 15]. It serves as foundation for Taylor mode to compute higher-order derivatives [e.g., 13, §13]: setting $x_1 = 1, x_2 = x_3 = 0$ yields $f_1 = \partial f(x_0), f_2 = \partial^2 f(x_0), f_3 = \partial^3 f(x_0)$. We call the univariate Taylor polynomial of a function $x(t)$ of degree K , represented by the coefficients (x_0, \dots, x_K) , the K -jet of x , following the terminology of JAX’s Taylor mode [2].

Notation for multivariate case. We consider the general case of computing higher-order derivatives, e.g. PDE operators, of a vector-to-vector function $\mathbf{f} : \mathbb{R}^D \rightarrow \mathbb{R}^C$. This requires additional notation to generalize eq. (1). Given K vectors $\mathbf{v}_1, \dots, \mathbf{v}_K \in \mathbb{R}^D$, we write their tensor product as

$$\otimes_{k=1}^K \mathbf{v}_k = \mathbf{v}_1 \otimes \dots \otimes \mathbf{v}_K \in (\mathbb{R}^D)^{\otimes K} \quad \text{with entries} \quad [\otimes_{k=1}^K \mathbf{v}_k]_{d_1, \dots, d_K} = [\mathbf{v}_1]_{d_1} \dots [\mathbf{v}_K]_{d_K}$$

for $d_1, \dots, d_K \in \{1, \dots, D\}$, and compactly write $\mathbf{v}^{\otimes K} = \otimes_{k=1}^K \mathbf{v}$. We define the inner product of two tensors $\mathbf{A}, \mathbf{B} \in (\mathbb{R}^D)^{\otimes K}$ as the Euclidean inner product of their flattened versions

$$\langle \mathbf{A}, \mathbf{B} \rangle := \sum_{d_1} \sum_{d_2} \dots \sum_{d_K} [\mathbf{A}]_{d_1, d_2, \dots, d_K} [\mathbf{B}]_{d_1, d_2, \dots, d_K} \in \mathbb{R}. \quad (2)$$

We allow broadcasting in eq. (2): if one tensor has more dimensions but matching trailing dimensions, we take the inner product for each component of the leading dimensions. This allows to express contractions with derivative tensors of vector-valued functions, e.g., contracting the k -th derivative tensor $\partial^k \mathbf{f}(x_0) \in \mathbb{R}^C \times (\mathbb{R}^D)^{\otimes k}$, such that $\langle \mathbf{A}, \partial^k \mathbf{f}(x_0) \rangle \in \mathbb{R}^C$.

Multivariate case & composition. Evaluating the K -jet of \mathbf{f} at $x_0 \in \mathbb{R}^D$ starts with the extension of x_0 to a smooth path $x : \mathbb{R} \rightarrow \mathbb{R}^D$ with $x(0) = x_0$. Formally, the K -jet of \mathbf{f} is defined as

$$J^K \mathbf{f} : \mathbb{R} \rightarrow \mathbb{R}^C, \quad (J^K \mathbf{f})(t) := \sum_{k=0}^K \frac{t^k}{k!} \mathbf{f}_k \quad \text{with} \quad \mathbf{f}_k := \frac{d^k}{dt^k} \mathbf{f}(x(t))|_{t=0}$$

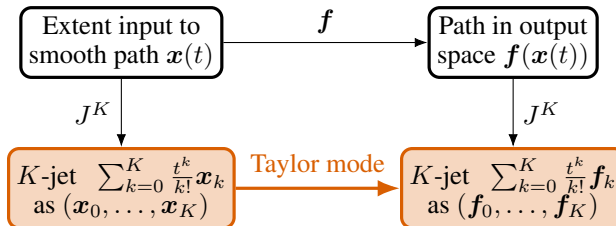


Figure 3: Taylor mode propagates Taylor coefficients of a path in input space. This results in the function-transformed path’s Taylor coefficients. The Taylor expansion of degree K is called a K -jet; hence Taylor mode propagates the input K -jet to the output K -jet.

and requires the K -jet of \mathbf{x} , $(J^K \mathbf{x})(t) := \sum_{k=0}^K \frac{t^k}{k!} \mathbf{x}_k$. As we are interested in the coefficients, we will slightly abuse the K -jet as mapping $(\mathbf{x}_0, \dots, \mathbf{x}_K) \mapsto (\mathbf{f}_0, \dots, \mathbf{f}_K)$ (see fig. 3 for an illustration).

As is common for AD, propagating the coefficients is broken down into composing \mathbf{f} of atomic functions with known derivatives and the chain rule. In the simplest case, let $\mathbf{f} = \mathbf{g} \circ \mathbf{h} : \mathbb{R}^D \rightarrow \mathbb{R}^I \rightarrow \mathbb{R}^C$ for two elemental functions \mathbf{g}, \mathbf{h} . Given the input K -jet for \mathbf{x} , the coefficients $\mathbf{h}_k = \frac{d^k}{dt^k} \mathbf{h}(\mathbf{x}(t))|_{t=0}$ follow from the generalized Faà di Bruno formula (spelled out for some k s in §A)

$$\mathbf{h}_k = \sum_{\sigma \in \text{part}(k)} \nu(\sigma) \left\langle \partial^{|\sigma|} \mathbf{h}, \otimes_{s \in \sigma} \mathbf{x}_s \right\rangle \quad \text{with} \quad \nu(\sigma) = \frac{k!}{(\prod_{s \in \sigma} n_s!) (\prod_{s \in \sigma} s!)} . \quad (3)$$

Here, $\text{part}(k)$ is the integer partitioning of k (a set of sets), ν is a multiplicity function, and n_s counts occurrences of s in a set σ (e.g. $n_1(\{1, 1, 3\}) = 2$ and $n_3 = 1$). Propagating the \mathbf{h}_k s through \mathbf{g} results in the K -jet for \mathbf{f} . In summary, the propagation scheme is (with $\mathbf{x}_k \in \mathbb{R}^D$, $\mathbf{h}_k \in \mathbb{R}^I$, $\mathbf{f}_k \in \mathbb{R}^C$)

$$\begin{aligned} \begin{pmatrix} \mathbf{x}_0 \\ \mathbf{x}_1 \\ \mathbf{x}_2 \\ \vdots \\ \mathbf{x}_K \end{pmatrix} &\xrightarrow{(3)} \begin{pmatrix} \mathbf{h}_0 = \mathbf{h}(\mathbf{x}_0) \\ \mathbf{h}_1 = \langle \partial \mathbf{h}(\mathbf{x}_0), \mathbf{x}_1 \rangle \\ \mathbf{h}_2 = \langle \partial^2 \mathbf{h}(\mathbf{x}_0), \mathbf{x}_1^{\otimes 2} \rangle + \langle \partial \mathbf{h}(\mathbf{x}_0), \mathbf{x}_2 \rangle \\ \vdots \\ \mathbf{h}_K = \sum_{\sigma \in \text{part}(K)} \nu(\sigma) \left\langle \partial^{|\sigma|} \mathbf{h}(\mathbf{x}_0), \otimes_{s \in \sigma} \mathbf{x}_s \right\rangle \end{pmatrix} \\ &\xrightarrow{(3)} \begin{pmatrix} \mathbf{g}_0 = \mathbf{g}(\mathbf{h}_0) \\ \mathbf{g}_1 = \langle \partial \mathbf{g}(\mathbf{h}_0), \mathbf{h}_1 \rangle \\ \mathbf{g}_2 = \langle \partial^2 \mathbf{g}(\mathbf{h}_0), \mathbf{h}_1^{\otimes 2} \rangle + \langle \partial \mathbf{g}(\mathbf{h}_0), \mathbf{h}_2 \rangle \\ \vdots \\ \mathbf{g}_K = \sum_{\sigma \in \text{part}(K)} \nu(\sigma) \left\langle \partial^{|\sigma|} \mathbf{g}(\mathbf{h}_0), \otimes_{s \in \sigma} \mathbf{h}_s \right\rangle \end{pmatrix} = \begin{pmatrix} \mathbf{f}_0 = \mathbf{f}(\mathbf{x}_0) \\ \mathbf{f}_1 = \langle \partial \mathbf{f}(\mathbf{x}_0), \mathbf{x}_1 \rangle \\ \mathbf{f}_2 = \langle \partial^2 \mathbf{f}(\mathbf{x}_0), \mathbf{x}_1^{\otimes 2} \rangle + \langle \partial \mathbf{f}(\mathbf{x}_0), \mathbf{x}_2 \rangle \\ \vdots \\ \mathbf{f}_K = \sum_{\sigma \in \text{part}(K)} \nu(\sigma) \left\langle \partial^{|\sigma|} \mathbf{f}(\mathbf{x}_0), \otimes_{s \in \sigma} \mathbf{x}_s \right\rangle \end{pmatrix} \end{aligned} \quad (4)$$

which describes the forward propagation of a *single* K -jet. However, computing popular PDE operators requires propagating *multiple* K -jets in parallel, then summing their results. We propose to pull this accumulation inside Taylor mode's propagation scheme, thereby collapsing it.

3 Collapsing Taylor Mode AD

We now describe how to collapse the Taylor mode AD computation of popular linear PDE operators and their stochastic approximations proposed in [26], and provide a general recipe for computing and collapsing general linear differential operators by interpolation, using earlier work from Griewank et al. [14]. At its core, our procedure uses the linearity of the highest Taylor coefficient's propagation rule. It allows to collapse coefficients along multiple directions and directly **propagate their sum**, rather than **propagating then summing**, yielding substantial reductions in computational cost.

3.1 Exploiting Linearity to Collapse Taylor Mode AD

To derive our proposed method, we start with a sum of K th-order directional derivatives of the function \mathbf{f} along R directions $\{\mathbf{v}_r\}_{r=1}^R$, which is a common building block for all our PDE operators:

$$\sum_{r=1}^R \langle \partial^K \mathbf{f}(\mathbf{x}_0), \mathbf{v}_r^{\otimes K} \rangle \in \mathbb{R}^C \quad (5)$$

(e.g. the exact Laplacian uses $K = 2$, $R = \dim(\mathbf{x}_0) = D$, and the unit vectors $\mathbf{v}_r = \mathbf{e}_r \in \mathbb{R}^D$ as directions; see §3.2 below). Instead of nesting K calls to 1st-order AD, we can use K -jets to calculate each summand of eq. (5) with Taylor mode. In total, we need R K -jets, and have to set the r -th jet's coefficients to $\mathbf{x}_{0,r} = \mathbf{x}_0$, $\mathbf{x}_{1,r} = \mathbf{v}_r$ and $\mathbf{x}_{2,r} = \dots = \mathbf{x}_{K,r} = \mathbf{0}$ (eq. (D13) applies this to eq. (4)).

Standard Taylor mode propagates $1 + KR$ vectors through every node of the computational graph (the 0th component is shared across all jets, see fig. 2). This gives the output jets $\{\{\mathbf{f}_{k,r}\}_{k=1}^K\}_{r=1}^R$, from which we only select the highest-degree coefficients $\{\mathbf{f}_{K,r}\}_{r=1}^R$, then sum them to obtain eq. (5).

The approach we propose here exploits that there is a special element in the set of integer partitions $\text{part}(K)$, namely the trivial partition $\tilde{\sigma} = \{K\}$, which contributes the term $\nu(\tilde{\sigma}) \langle \partial \mathbf{g}(\mathbf{h}_0), \mathbf{h}_{K,r} \rangle$ to

eq. (3). This is the only term that uses the input jet's highest coefficient $\mathbf{h}_{K,r}$, and its dependency is *linear*. Separating it in the highest coefficient's forward propagation, we get (using $\nu(\tilde{\sigma}) = 1$)

$$\sum_{r=1}^R \mathbf{f}_{K,r} = \sum_{r=1}^R \mathbf{g}_{K,r} = \sum_{r=1}^R \sum_{\sigma \in \text{part}(K) \setminus \{\tilde{\sigma}\}} \nu(\sigma) \left\langle \partial^{|\sigma|} \mathbf{g}(\mathbf{h}_0), \bigotimes_{s \in \sigma} \mathbf{h}_{K,r} \right\rangle + \sum_{r=1}^R \langle \partial \mathbf{g}(\mathbf{h}_0), \mathbf{h}_{K,r} \rangle$$

and since the propagation rule is linear w.r.t. $\mathbf{h}_{K,r}$, we can pull the summation inside:

$$\sum_{r=1}^R \mathbf{g}_{K,r} = \sum_{r=1}^R \sum_{\sigma \in \text{part}(K) \setminus \{\tilde{\sigma}\}} \nu(\sigma) \left\langle \partial^{|\sigma|} \mathbf{g}(\mathbf{h}_0), \bigotimes_{s \in \sigma} \mathbf{h}_{K,r} \right\rangle + \left\langle \partial \mathbf{g}(\mathbf{h}_0), \sum_{r=1}^R \mathbf{h}_{K,r} \right\rangle. \quad (6)$$

This is the key insight of our work: *The summed highest-degree output coefficients depend on the summed highest-degree input coefficients* (as well as all lower-degree coefficients). The reason is *linearity* in Faà di Bruno's formula. Hence, to compute the sum $\sum_r \mathbf{g}_{K,r}$ we can directly propagate the sum $\sum_r \mathbf{h}_{K,r}$, collapsing coefficients over all directions. We call this *collapsed Taylor mode AD*.

Collapsed Taylor mode propagates only $1 + (K - 1)R + 1$ vectors through every node in the computational graph (see fig. 2 and eq. (D14) which applies this to eq. (3)). These savings of $R - 1$ coefficients are significant improvements over standard Taylor mode, as we show below. In the following, we discuss how to collapse the Taylor mode computation of various PDE operators.

3.2 Linear Second-order Operators

Laplacian. The Laplace operator plays a central role in Physics and engineering, including electrostatics, fluid dynamics, heat conduction, and quantum mechanics [10, 23]. It contains the Hessian trace of each element of a function, i.e., for $\mathbf{f} : \mathbb{R}^D \rightarrow \mathbb{R}^C$, it is

$$\underbrace{\Delta \mathbf{f}(\mathbf{x}_0)}_{\in \mathbb{R}^C} := \langle \partial^2 \mathbf{f}(\mathbf{x}_0), \mathbf{I}_D \rangle \quad \begin{cases} = \sum_{d=1}^D \langle \partial^2 \mathbf{f}(\mathbf{x}_0), \mathbf{e}_d^{\otimes 2} \rangle & \text{(exact)} \\ \stackrel{[26]}{\approx} \frac{1}{S} \sum_{s=1}^S \langle \partial^2 \mathbf{f}(\mathbf{x}_0), \mathbf{v}_s^{\otimes 2} \rangle & \text{(stochastic)} \end{cases} \quad (7a)$$

with the d -th standard basis vector \mathbf{e}_d used for exact computation, and S random vectors \mathbf{v}_s drawn i.i.d. from a distribution with unit variance (e.g. Rademacher or standard Gaussian) for stochastic estimation. By pattern-matching eq. (7a) with eq. (5) we conclude that $K = 2$, and the following choices for computing the Laplacian with standard Taylor mode:

$$\begin{aligned} \{(\mathbf{x}_{0,d} = \mathbf{x}_0, \quad \mathbf{x}_{1,d} = \mathbf{e}_d, \quad \mathbf{x}_{2,d} = \mathbf{0})\}_{d=1}^D & \quad \mathbf{1} + D + D \text{ vectors} \quad \text{(exact)} \\ \{(\mathbf{x}_{0,s} = \mathbf{x}_0, \quad \mathbf{x}_{1,s} = \mathbf{v}_s, \quad \mathbf{x}_{2,s} = \mathbf{0})\}_{s=1}^S & \quad \mathbf{1} + S + S \text{ vectors} \quad \text{(stochastic)} \end{aligned} \quad (7b)$$

Collapsing standard Taylor mode yields $\mathbf{1} + D + \mathbf{1}$ (exact) and $\mathbf{1} + S + \mathbf{1}$ (stochastic) vectors. In fact, the collapsed Taylor mode for the exact Laplacian is the forward Laplacian from Li et al. [20] (see eq. (D16) for detailed presentation of the forward propagation). Note how we can seamlessly also collapse the stochastic approximation over the sampled directions, which is currently not done.

Weighted Laplacian. A natural generalization of the Laplacian involves contracting with a positive semi-definite matrix $\mathbf{D} = \boldsymbol{\sigma} \boldsymbol{\sigma}^\top \in \mathbb{R}^{D \times D}$ rather than the identity. \mathbf{D} may represent the diffusion tensor in Kolmogorov-type PDEs like the Fokker-Planck equation [17], and $\boldsymbol{\sigma}$ can depend on \mathbf{x}_0 [8]. The weighted Laplacian contains the weighted Hessian's trace $\text{Tr}(\boldsymbol{\sigma} \boldsymbol{\sigma}^\top \partial^2 [\mathbf{f}]_c)$ for each output element c of \mathbf{f} . If $\text{rank}(\mathbf{D}) = R$ and therefore $\boldsymbol{\sigma} = (\mathbf{s}_1, \dots, \mathbf{s}_R) \in \mathbb{R}^{D \times R}$, it is

$$\underbrace{\Delta_{\mathbf{D}} \mathbf{f}(\mathbf{x}_0)}_{\in \mathbb{R}^C} := \langle \partial^2 \mathbf{f}(\mathbf{x}_0), \mathbf{D} \rangle \quad \begin{cases} = \sum_{r=1}^R \langle \partial^2 \mathbf{f}(\mathbf{x}_0), \mathbf{s}_r^{\otimes 2} \rangle & \text{(exact)} \\ \stackrel{[17]}{\approx} \frac{1}{S} \sum_{s=1}^S \langle \partial^2 \mathbf{f}(\mathbf{x}_0), (\boldsymbol{\sigma} \mathbf{v}_s)^{\otimes 2} \rangle & \text{(stochastic)} \end{cases} \quad (8a)$$

Computing it requires evaluating the following 2-jets with standard Taylor mode:

$$\begin{aligned} \{(\mathbf{x}_{0,r} = \mathbf{x}_0, \quad \mathbf{x}_{1,r} = \mathbf{s}_r, \quad \mathbf{x}_{2,r} = \mathbf{0})\}_{r=1}^R & \quad \mathbf{1} + R + R \text{ vectors} \quad \text{(exact)} \\ \{(\mathbf{x}_{0,s} = \mathbf{x}_0, \quad \mathbf{x}_{1,s} = \boldsymbol{\sigma} \mathbf{v}_s, \quad \mathbf{x}_{2,s} = \mathbf{0})\}_{s=1}^S & \quad \mathbf{1} + S + S \text{ vectors} \quad \text{(stochastic)} \end{aligned} \quad (8b)$$

Our collapsed Taylor mode uses $\mathbf{1} + R + \mathbf{1}$ (exact) and $\mathbf{1} + S + \mathbf{1}$ (stochastic) vectors. This yields the modified forward Laplacian from Li et al. [19]; collapsing the stochastic variant speeds up the Hutchinson trace estimator from Hu et al. [17]. For indefinite \mathbf{D} , we can simply apply this scheme to the positive and negative eigen-spaces (however, such weightings are not used in practise).

3.3 Collapsed Taylor Mode for Arbitrary Mixed Partial Derivatives

So far, we discussed operators that result from contracting the second-order derivative tensor with a coefficient matrix (\mathbf{I} or \mathbf{D}) that can conveniently be written as sum of vector outer products. For orders higher than two, the coefficient tensor can in general *not* easily be decomposed as such. Hence, we extend our framework to also cover differential operators containing mixed-partial derivatives by evaluating a suitable family of jets using the interpolation result of Griewank et al. [14]. As illustrative example, we will use the biharmonic operator with a 4-dimensional coefficient tensor:

$$\Delta^2 \mathbf{f}(\mathbf{x}_0) \quad \begin{cases} = \sum_{d_1=1}^D \sum_{d_2=1}^D \langle \partial^4 \mathbf{f}(\mathbf{x}_0), \mathbf{e}_{d_1}^{\otimes 2} \otimes \mathbf{e}_{d_2}^{\otimes 2} \rangle & \text{(exact)} \\ \stackrel{[26]}{\approx} \frac{D}{S} \sum_{s=1}^S \langle \partial^4 \mathbf{f}(\mathbf{x}_0), \mathbf{v}_s^{\otimes 4} \rangle & \text{(stochastic)} \end{cases} \quad (9)$$

We can directly collapse the stochastic version: draw S standard normal vectors $\mathbf{v}_1, \dots, \mathbf{v}_S$ and propagate the coefficients $\{(\mathbf{x}_{0,s} = \mathbf{x}_0, \mathbf{x}_{1,s} = \mathbf{v}_s, \mathbf{x}_{2,s} = \mathbf{x}_{3,s} = \mathbf{x}_{4,s} = \mathbf{0})\}_{s=1}^S$. With standard Taylor mode, this uses $1 + 4S$ vectors; collapsed Taylor mode uses $1 + 3S + 1$ vectors. For the exact biharmonic operator, however, we need to develop an approach to compute mixed partials.

General approach. Assume we want to compute a linear differential operator of degree K . We can do so by contracting the K -th order derivative tensor $\partial^K \mathbf{f}(\mathbf{x}_0)$ with a coefficient tensor $\mathbf{C} \in (\mathbb{R}^D)^{\otimes K}$. We can always express this tensor in a tensor product basis, such that

$$\langle \partial^K \mathbf{f}(\mathbf{x}_0), \mathbf{C} \rangle = \sum_{d_1=1}^{D_1} \dots \sum_{d_I=1}^{D_I} \langle \partial^K \mathbf{f}(\mathbf{x}_0), \mathbf{v}_{d_1}^{\otimes i_1} \otimes \dots \otimes \mathbf{v}_{d_I}^{\otimes i_I} \rangle \in \mathbb{R}^C, \quad (10)$$

where the multi-index entries $\mathbf{i} = (i_1, \dots, i_I)$ sum to K and $D_j \leq D$. For the exact biharmonic operator (eq. (9)), we identify $K = 4, I = 2, \mathbf{i} = (2, 2), D_1 = D_2 = D, \mathbf{v}_{d_1} = \mathbf{e}_{d_1}$, and $\mathbf{v}_{d_2} = \mathbf{e}_{d_2}$. From the Faà di Bruno formula, we know that we can only compute terms of the form $\langle \partial^K \mathbf{f}(\mathbf{x}_0), \mathbf{v}^{\otimes K} \rangle$ with a K -jet. The challenge in eq. (10) is that it includes terms where *not* all directions coincide (e.g. for the biharmonic we have $I = 2$ different directions).

Fortunately, Griewank et al. [14] derived an approach to reconstruct such mixed-direction terms by linearly combining a *family* of K -jets that is determined by all vectors $\mathbf{j} \in \mathbb{N}^I$ whose entries sum to K , see fig. 4 for an illustration for the biharmonic (5 members). The K -jets along these directions are then combined with coefficients $\gamma_{\mathbf{i}, \mathbf{j}} \in \mathbb{R}$, whose definition we provide in §E. In summary, we get

$$\langle \partial^K \mathbf{f}(\mathbf{x}_0), \mathbf{v}_{d_1}^{\otimes i_1} \otimes \dots \otimes \mathbf{v}_{d_I}^{\otimes i_I} \rangle = \sum_{\mathbf{j} \in \mathbb{N}^I, \|\mathbf{j}\|_1 = K} \frac{\gamma_{\mathbf{i}, \mathbf{j}}}{K!} \left\langle \partial^K \mathbf{f}(\mathbf{x}_0), \left(\sum_{i=1}^I \mathbf{v}_{d_i} [\mathbf{j}]_i \right)^{\otimes K} \right\rangle. \quad (11)$$

This construction allows us to rewrite eq. (10) as

$$\sum_{d_1=1}^{D_1} \dots \sum_{d_I=1}^{D_I} \sum_{\mathbf{j} \in \mathbb{N}^I, \|\mathbf{j}\|_1 = K} \frac{\gamma_{\mathbf{i}, \mathbf{j}}}{K!} \left\langle \partial^K \mathbf{f}(\mathbf{x}_0), \left(\sum_{i=1}^I \mathbf{v}_{d_i} [\mathbf{j}]_i \right)^{\otimes K} \right\rangle,$$

and—since the coefficients $\gamma_{\mathbf{i}, \mathbf{j}}$ only depend on the problem structure (K, I and \mathbf{i}) and *not* on the function \mathbf{f} and the directions \mathbf{v}_{d_i} [14]—we can pull out the inner sum to obtain the final expression

$$\sum_{\mathbf{j} \in \mathbb{N}^I, \|\mathbf{j}\|_1 = K} \frac{\gamma_{\mathbf{i}, \mathbf{j}}}{K!} \sum_{d_1=1}^{D_1} \dots \sum_{d_I=1}^{D_I} \left\langle \partial^K \mathbf{f}(\mathbf{x}_0), \left(\sum_{i=1}^I \mathbf{v}_{d_i} [\mathbf{j}]_i \right)^{\otimes K} \right\rangle. \quad (12)$$

We can evaluate eq. (12) with standard Taylor mode: For each \mathbf{j} , compute $\prod_{i=1}^I D_i$ K -jets with coefficients $\mathbf{x}_0, \mathbf{x}_1 = \sum_i \mathbf{v}_{d_i} [\mathbf{j}]_i, \mathbf{x}_2 = \dots = \mathbf{x}_K = \mathbf{0}$. The sums from the tensor basis expansion can be collapsed with our proposed optimization, removing $\prod_{i=1}^I D_i$ vectors from the propagation for each \mathbf{j} . After repeating for each member \mathbf{j} of the interpolation family, we form the linear combination using the $\gamma_{\mathbf{i}, \mathbf{j}}$ s, which yields the desired differential operator. We can often exploit symmetries in the $\gamma_{\mathbf{i}, \mathbf{j}}$ s and basis vectors to further reduce the number of K -jets (see §E.1 for a complete example).

Applied to the biharmonic operator. Let us now illustrate the key steps of applying eq. (12) to the exact biharmonic operator eq. (9) (full procedure in §E.1). Figure 4 illustrates the 5 multi-indices \mathbf{j} characterizing the 4-jets we need to interpolate $\langle \partial^4 \mathbf{f}(\mathbf{x}_0), \mathbf{e}_{d_1}^{\otimes 2} \otimes \mathbf{e}_{d_2}^{\otimes 2} \rangle$, and their coefficients $\gamma_{\mathbf{i}, \mathbf{j}}$.

Their definition, see eq. (E17), shows the equality of $\gamma_{i,j}$ for $j = (4, 0)$ and $j = (0, 4)$, as well as $j = (3, 1)$ and $j = (1, 3)$. Exploiting those symmetries reduces the number of interpolation terms from 5 to 3 (eq. (E20)), corresponding to $D + D^2 + D^2$ 4-jets. Removing doubly-computed terms brings down the number of 4-jets to $D + D(D-1) + \frac{1}{2}D(D-1)$ (eq. (E22)). Translated to vectors, standard Taylor mode propagates $1 + 4D + 4D(D-1) + \frac{1}{2}D(D-1) = 6D^2 - 2D + 1$ vectors. After collapsing, we get $1 + 3D + 1 + 3D(D-1) + 1 + \frac{3}{2}D(D-1) + 1 = \frac{9}{2}D^2 - \frac{3}{2}D + 4$ vectors. This demonstrates the relevance of collapsing: it achieves a 25 % reduction in the quadratic coefficient.

Summary & relation to other approaches for computing mixed partials. The scheme we propose based on Griewank et al. [14]’s interpolation result allows to calculate *general* linear differential operators beyond Laplacians, and is amenable to collapsing. Admittedly, eq. (12) seems daunting at first glance. However, it (i) offers a one-fits-all recipe to construct schemes for general linear PDE operators, and (ii) does not use jets of order $K' > K$ to compute K -th order derivatives. It is possible to derive more “pedagogical” approaches, which however require hand-crafted interpolation rules case by case, and propagation of higher-order jets which is costly (see §E.2 for a pedagogical example using less efficient 6-jets to compute the biharmonic operator, or [26, §F] for other operators).

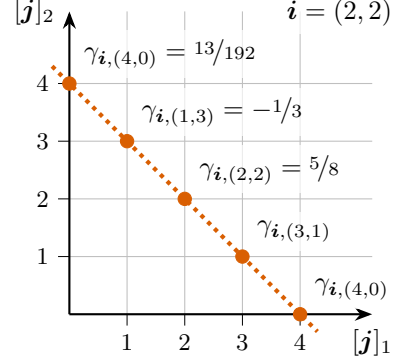


Figure 4: **Illustration of eq. (12) for the biharmonic operator**, i.e. the 5 values of j with $\|j\|_1 = 4$ and their coefficients $\gamma_{i,j}$ to interpolate the desired mixed partials.

4 Implementation & Experiments

Here, we describe our implementation of the Taylor mode collapsing process and empirically validate its performance improvements on the previously discussed operators.

Design decisions & limitations. JAX [3] already offers an—albeit experimental—Taylor mode implementation [2]. However, we found it challenging to capture the computation graph and modify it using JAX’s public interface. In contrast, PyTorch [21] provides `torch.fx` [25], which offers a user-friendly interface to capture and transform computational graphs purely in Python. Hence, we re-implemented Taylor mode in PyTorch, taking heavy inspiration from the JAX implementation.

This deliberate choice imposes certain limitations. First, as of now, our Taylor mode in PyTorch supports only a small number of primitives, because the Taylor arithmetic in eq. (3) needs to be implemented case by case (this of course also applies to JAX’s Taylor mode, which has broader operator coverage). Second, while our Taylor mode implementation is competitive with JAX’s, we did not fully optimize it (e.g. we do *not* use in-place operations, and we do *not* implement the efficient schemes from Griewank & Walther [13, §13], but stick to Faà di Bruno (eq. (3))). Given our implementation’s superiority compared to nested first-order AD that we demonstrate below, these are promising future efforts that will further improve performance, and we believe that making Taylor mode available to the PyTorch community is also an important step towards establishing its use.

Usage (overview in §B). Our implementation takes a PyTorch function (e.g. a neural net) and first captures its computational graph using `torch.fx`’s symbolic tracing mechanism. Then, it replaces each operation with its Taylor arithmetic, which yields the computational graph of the function’s K -jet. Users can then write a function to compute their differential operator with this vanilla Taylor mode. Collapsing is achieved using a function `simplify`, which traces the computation again, rewrites the graph, and propagates the summation of highest coefficients up to its leafs. This requires one backward traversal through the graph (§C presents a detailed example). The simplified graph produces the same result, but propagates summed coefficients, i.e. uses collapsed Taylor mode.

Experimental setup. We empirically validate our proposed collapsing approach in PyTorch. We compare **standard Taylor mode** with **collapsed Taylor mode** and **nested 1st-order AD** on an Nvidia RTX 6000 GPU with 24 GiB memory. To implement the (weighted) Laplacian and its stochastic counterpart, we use vector-Hessian-vector products (VHVPs) in forward-over-reverse order, as

recommended [5, 13]. For the biharmonic operator, we simply nest two VHVPs. For the weighted Laplacian’s coefficient matrix, we choose a full-rank diagonal matrix. To avoid confounding factors, all implementations are executed without compilation (our JAX experiments with the Laplacian in §G confirm that `jit` does not affect the relative performance). As common for PINNs [e.g. 6, 26], we use a 5-layer MLP $f_\theta : D \rightarrow 768 \rightarrow 768 \rightarrow 512 \rightarrow 512 \rightarrow 1$ with \tanh activations and trainable parameters θ , and compute the PDE operators on batches of size N . We measure three performance metrics: (1) **runtime** reports the smallest execution time of 50 repetitions. (2) **Peak memory (non-differentiable)** measures the maximum allocated GPU memory when computing the PDE operator’s value (e.g. used in VMC [23]) inside a `torch.no_grad` context. (3) **Peak memory (differentiable)** is the maximum memory usage when computing the PDE operator inside a `torch.enable_grad` context, which allows backpropagation to θ (required for training PINNs, or alternative VMC works [29, 31]). This demands saving intermediates, which uses more memory but does not affect runtime. As memory allocation does not fluctuate much, we measure it in a single run.

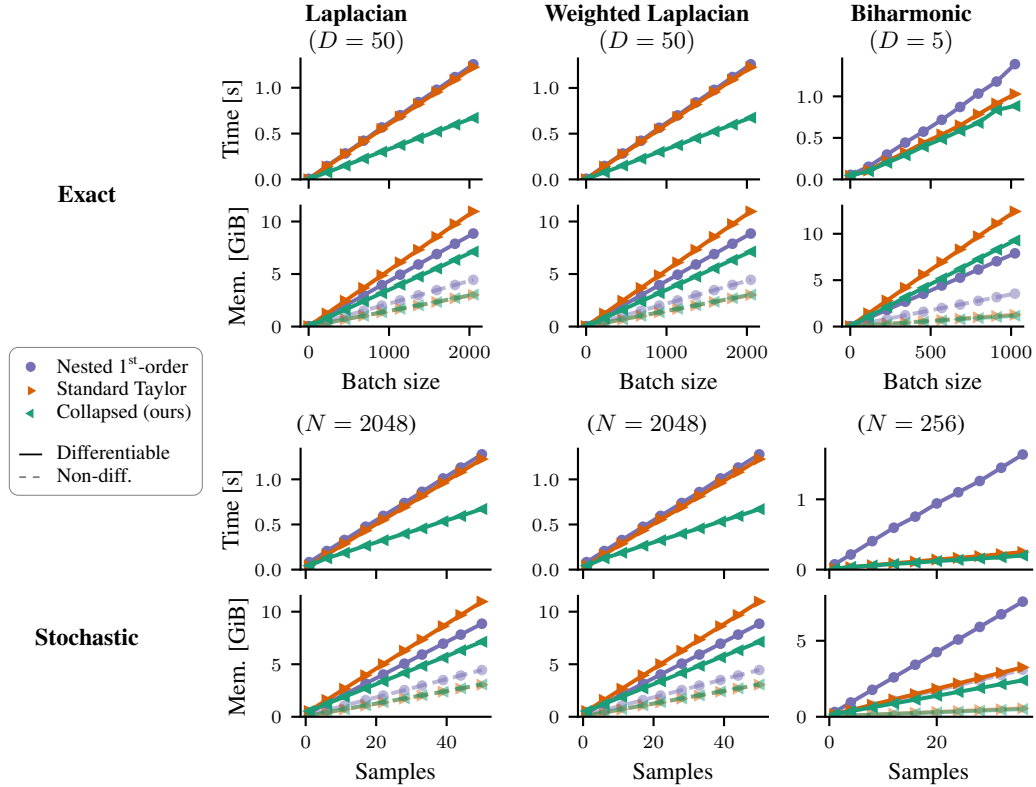


Figure 5: **Collapsed Taylor mode accelerates standard Taylor mode and outperforms nested 1st-order AD.** Exact computation varies the batch size, stochastic computation fixes a batch size and varies the samples such that $S < D$ (Laplacians), and $2 + 3S < 9/2D^2 - 3/2D + 4$ (biharmonic operator); we could compute exactly otherwise. Opaque markers are non-differentiable computations.

²For the exact biharmonic, the 1st-order AD implementation—unlike our Taylor mode implementations—has a somewhat unfair advantage: it leverages the operator’s special structure by computing it as the Laplacian of the Laplacian, $\Delta^2 f(x_0) = \Delta(\Delta f(x_0))$. Had we instead naively computed, then summed, the fourth-order derivatives by tensor-vector-products (TVPs) with $\partial^4 f(x_0)$ [e.g. done in 17], performance would have degraded *dramatically*, similar to the performance gap we observe for the stochastic biharmonic operator which has to use these TVPs. Hence, we omit this naive exact approach, which, however, is *necessary for general operators*.

We chose the biharmonic as a case study for a general linear differential operator to show that even here, collapsing Taylor yields improvements, despite increased memory use. In §G, we confirm that incorporating this advantage by nesting Laplacians—also possible in (collapsed) Taylor mode—offers the most efficient approach, achieving roughly 3x better runtime and memory with our collapsing technique (table G3 and fig. G9).

Results. Figure 5 visualizes the growth in computational resources w.r.t. the batch size (exact) and random samples (stochastic) for fixed dimensions D . Runtime and memory increase linearly in both, as expected. We quantify the results by fitting linear functions and reporting their slopes (i.e., time and memory added per datum/sample) in table 1. We make the following observations:

- **Collapsed Taylor mode accelerates standard Taylor mode.** The measured performance differences correspond well with the theoretical estimate from counting the number of forward-propagated vectors. E.g., for the exact Laplacian, adding one datum introduces $2 + D$ versus $1 + 2D$ new vectors. For $D = 50$, their ratio is $(2+D)/(1+2D) \approx 0.51$. Empirically, we measure that adding one datum adds **0.60 ms** to standard, and **0.33 ms** to collapsed, Taylor mode; the ratio of ≈ 0.55 is close. Similar arguments hold for peak memory of differentiable computation, stochastic approximation, and the other PDE operators (see table F2 for all comparisons).
- **Collapsed Taylor mode outperforms nested 1st-order AD.** For the exact and stochastic (weighted) Laplacians, collapsed Taylor mode is roughly twice as fast (consistent with the JAX results in fig. 1) while using only 70-80% memory. For the biharmonic operator, we also observe speed-ups; in the stochastic case up to 9x in time, and 3x in memory (differentiable).

Comparison with JAX. We also conducted experiments with JAX (+ `jit`) to rule out artifacts from choosing PyTorch, implementation mistakes in our Taylor mode library, or unexpected simplifications from the JIT compiler. We find that the choice of ML framework does not affect the results. E.g., when computing the exact Laplacian with nested first-order AD, PyTorch consumes 0.61 ms per datum (table 1), while JAX uses 0.57 ms (fig. 1 and table G3). We find the same trend when comparing our collapsed Taylor mode and JAX’s forward Laplacian. Interestingly, we noticed that JAX’s Taylor mode was consistently slower than our PyTorch implementation, despite using `jit`. We conclude from these results that (both ours, as well as the existing JAX) Taylor mode still has potential for improvements that may further increase the margin to nested first-order.

Table 1: **Benchmark from fig. 5 in numbers.** We fit linear functions and report their slopes, i.e., how much runtime and memory increase when incrementing the batch size or random samples. We show two significant digits and bold values are best according to parenthesized values.

Mode	Per-datum or -sample cost	Implementation	Laplacian	Weighted Laplacian	Biharmonic
Exact	Time [ms]	Nested 1 st -order	0.61 (1.0x)	0.61 (1.0x)	1.3 (1.0x)
		Standard Taylor	0.60 (0.98x)	0.60 (0.98x)	0.98 (0.76x)
		Collapsed (ours)	0.33 (0.54x)	0.33 (0.54x)	0.86 (0.66x)
	Mem. [MiB] (differentiable)	Nested 1 st -order	4.4 (1.0x)	4.4 (1.0x)	7.9 (1.0x) ²
		Standard Taylor	5.5 (1.2x)	5.5 (1.2x)	12 (1.6x)
		Collapsed (ours)	3.6 (0.81x)	3.6 (0.81x)	9.3 (1.2x)
Stochastic	Time [ms]	Nested 1 st -order	2.2 (1.0x)	2.2 (1.0x)	3.5 (1.0x)
		Standard Taylor	1.5 (0.68x)	1.5 (0.68x)	1.3 (0.36x)
		Collapsed (ours)	1.5 (0.68x)	1.5 (0.68x)	1.1 (0.33x)
	Mem. [MiB] (differentiable)	Nested 1 st -order	24 (1.0x)	24 (1.0x)	44 (1.0x)
		Standard Taylor	24 (0.99x)	24 (0.99x)	6.7 (0.15x)
		Collapsed (ours)	13 (0.52x)	13 (0.51x)	5.1 (0.12x)
	Mem. [MiB] (non-diff.)	Nested 1 st -order	180 (1.0x)	180 (1.0x)	210 (1.0x)
		Standard Taylor	220 (1.2x)	220 (1.2x)	90 (0.42x)
		Collapsed (ours)	140 (0.78x)	140 (0.78x)	65 (0.31x)
	Mem. [MiB] (non-diff.)	Nested 1 st -order	89 (1.0x)	89 (1.0x)	86 (1.0x)
		Standard Taylor	61 (0.69x)	61 (0.69x)	15 (0.17x)
		Collapsed (ours)	62 (0.69x)	62 (0.69x)	14 (0.16x)

5 Conclusion

Computing differential operators is a critical component in scientific machine learning, particularly for Physics-informed neural networks and variational Monte Carlo. Our work introduces collapsed Taylor mode, a simple yet effective optimization based on linearity in Faà di Bruno’s formula, that propagates the sum of highest-order Taylor coefficients, rather than propagating then summing. It contains recent advances in forward-mode schemes, recovering the forward Laplacian [20], while being applicable to stochastic Taylor mode [17, 26]. We demonstrated that collapsed Taylor mode is useful to compute general linear differential operators, leveraging Griewank et al. [14]’s interpolation formula. Empirically, we confirmed speed-ups and memory savings for computing (randomized) Laplacians and biharmonic operators after collapsing Taylor mode, in accordance with our theoretical analysis, and confirmed its superiority to nesting first-order automatic differentiation. As the optimizations are achieved through simple graph rewrites based on linearity, we believe they could be integrated into existing just-in-time compilers without requiring a new interface or burdening users.

Our work takes an important step towards making Taylor mode a practical alternative to nested first-order differentiation in scientific machine learning, while maintaining ease of use. Future work could focus on integrating these optimizations directly into ML compilers, broadening operator coverage of our PyTorch implementation, and exploring additional graph optimizations for AD.

Acknowledgments and Disclosure of Funding

Resources used in preparing this research were provided, in part, by the Province of Ontario, the Government of Canada through CIFAR, and companies sponsoring the Vector Institute. The research was funded partly by the DFG under Germany’s Excellence Strategy – The Berlin Mathematics Research Center MATH+ (EXC-2046/1, project ID:390685689). M.Z. acknowledges support from an ETH Postdoctoral Fellowship for the project “Reliable, Efficient, and Scalable Methods for Scientific Machine Learning”.

References

- [1] Arbogast, L. *Du calcul des dérivations*. 1800.
- [2] Bettencourt, J., Johnson, M. J., and Duvenaud, D. Taylor-mode automatic differentiation for higher-order derivatives in JAX. In *Advances in Neural Information Processing Systems (NeurIPS); Workshop on Program Transformations for ML*, 2019.
- [3] Bradbury, J., Frostig, R., Hawkins, P., Johnson, M. J., Leary, C., Maclaurin, D., and Wanderman-Milne, S. JAX: composable transformations of Python+NumPy programs, 2018.
- [4] Carleo, G. and Troyer, M. Solving the quantum many-body problem with artificial neural networks. *Science*, 355(6325):602–606, 2017.
- [5] Dagr  ou, M., Ablin, P., Vaiter, S., and Moreau, T. How to compute Hessian-vector products? In *International Conference on Learning Representations (ICLR) Blogposts*, 2024.
- [6] Dangel, F., M  ller, J., and Zeinhofer, M. Kronecker-factored approximate curvature for physics-informed neural networks. In *Advances in Neural Information Processing Systems (NeurIPS)*, 2024.
- [7] Dwivedi, V. and Srinivasan, B. Solution of biharmonic equation in complicated geometries with physics informed extreme learning machine. *Journal of Computing and Information Science in Engineering*, 20(6), 05 2020. ISSN 1530-9827.
- [8] Fa, K. S. Solution of Fokker-Planck equation for a broad class of drift and diffusion coefficients. *Phys. Rev. E*, 2011.
- [9] Fa   Di Bruno, F. Note sur une nouvelle formule de calcul diff  rentiel. *Quarterly J. Pure Appl. Math*, 1857.
- [10] Foulkes, W. M., Mitas, L., Needs, R., and Rajagopal, G. Quantum Monte Carlo simulations of solids. *Reviews of Modern Physics*, 73(1):33, 2001.

- [11] Fraenkel, L. Formulae for high derivatives of composite functions. In *Mathematical Proceedings of the Cambridge Philosophical Society*, 1978.
- [12] Gao, N., Köhler, J., and Foster, A. folx - forward Laplacian for JAX, 2023. URL <http://github.com/microsoft/folx>.
- [13] Griewank, A. and Walther, A. *Evaluating derivatives: principles and techniques of algorithmic differentiation*. SIAM, 2008.
- [14] Griewank, A., Utke, J., and Walther, A. Evaluating higher derivative tensors by forward propagation of univariate Taylor series. *Mathematics of Computation*, 69, 1999.
- [15] Hardy, M. Combinatorics of partial derivatives, 2006. arXiv.
- [16] Hermann, J., Schätzle, Z., and Noé, F. Deep-neural-network solution of the electronic Schrödinger equation. *Nature Chemistry*, 12(10):891–897, 2020.
- [17] Hu, Z., Shi, Z., Karniadakis, G. E., and Kawaguchi, K. Hutchinson trace estimation for high-dimensional and high-order physics-informed neural networks. 2023.
- [18] Karniadakis, G. E., Kevrekidis, I. G., Lu, L., Perdikaris, P., Wang, S., and Yang, L. Physics-informed machine learning. *Nature Reviews Physics*, 3(6):422–440, 2021.
- [19] Li, R., Wang, C., Ye, H., He, D., and Wang, L. DOF: Accelerating high-order differential operators with forward propagation. In *International Conference on Learning Representations (ICLR), Workshop on AI4DifferentialEquations In Science*, 2024.
- [20] Li, R., Ye, H., Jiang, D., Wen, X., Wang, C., Li, Z., Li, X., He, D., Chen, J., Ren, W., et al. A computational framework for neural network-based variational Monte Carlo with forward Laplacian. *Nature Machine Intelligence*, 2024.
- [21] Paszke, A., Gross, S., Massa, F., Lerer, A., Bradbury, J., Chanan, G., Killeen, T., Lin, Z., Gimelshein, N., Antiga, L., Desmaison, A., Kopf, A., Yang, E., DeVito, Z., Raison, M., Tejani, A., Chilamkurthy, S., Steiner, B., Fang, L., Bai, J., and Chintala, S. PyTorch: An imperative style, high-performance deep learning library. In *Advances in Neural Information Processing Systems (NeurIPS)*. 2019.
- [22] Pearlmutter, B. A. Fast exact multiplication by the Hessian. *Neural Computation*, 1994.
- [23] Pfau, D., Spencer, J. S., Matthews, A. G., and Foulkes, W. M. C. Ab initio solution of the many-electron Schrödinger equation with deep neural networks. *Physical Review Research*, 2020.
- [24] Raissi, M., Perdikaris, P., and Karniadakis, G. E. Physics-informed neural networks: A deep learning framework for solving forward and inverse problems involving nonlinear partial differential equations. *Journal of Computational physics*, 378:686–707, 2019.
- [25] Reed, J., DeVito, Z., He, H., Ussery, A., and Ansel, J. torch.fx: Practical program capture and transformation for deep learning in python. *Proceedings of Machine Learning and Systems (MLSys)*, 2022.
- [26] Shi, Z., Hu, Z., Lin, M., and Kawaguchi, K. Stochastic Taylor derivative estimator: Efficient amortization for arbitrary differential operators. In *Advances in Neural Information Processing Systems (NeurIPS)*, 2024.
- [27] Sun, J., Berner, J., Richter, L., Zeinhofer, M., Müller, J., Azizzadenesheli, K., and Anandkumar, A. Dynamical measure transport and neural PDE solvers for sampling. *arXiv preprint arXiv:2407.07873*, 2024.
- [28] Sun, R., Li, D., Liang, S., Ding, T., and Srikant, R. The global landscape of neural networks: An overview, 2020.
- [29] Toulouse, J. and Umrigar, C. J. Optimization of quantum Monte Carlo wave functions by energy minimization. *The Journal of Chemical Physics (JCP)*, 2007.

- [30] Vahab, M., Haghighat, E., Khaleghi, M., and Khalili, N. A physics-informed neural network approach to solution and identification of biharmonic equations of elasticity. *Journal of Engineering Mechanics*, 148(2), 2022.
- [31] Webber, R. J. and Lindsey, M. Rayleigh-Gauss-Newton optimization with enhanced sampling for variational Monte Carlo. *Physical Review Research*, 2022.

Collapsing Taylor Mode Automatic Differentiation (Supplementary Material)

A	Faà Di Bruno Formula Cheat Sheet	14
B	Visual Tour: From Function to Collapsed Taylor Mode	15
C	Graph Simplifications	16
D	Exploiting Linearity to Collapse Taylor Mode	19
	D.1 Second-order Operators — Laplacian	20
E	Details on (Collapsed) Taylor Mode for Arbitrary Mixed Partial Derivatives	21
	E.1 Applied to the Biharmonic Operator	21
	E.2 Pedagogical Approach for the Biharmonic Operator with 6-jets	22
F	PyTorch Benchmark	23
G	JAX Benchmark	23

To give some intuition on the Faà di Bruno formula, we illustrate eq. (4) for higher orders here:

14

B Visual Tour: From Function to Collapsed Taylor Mode

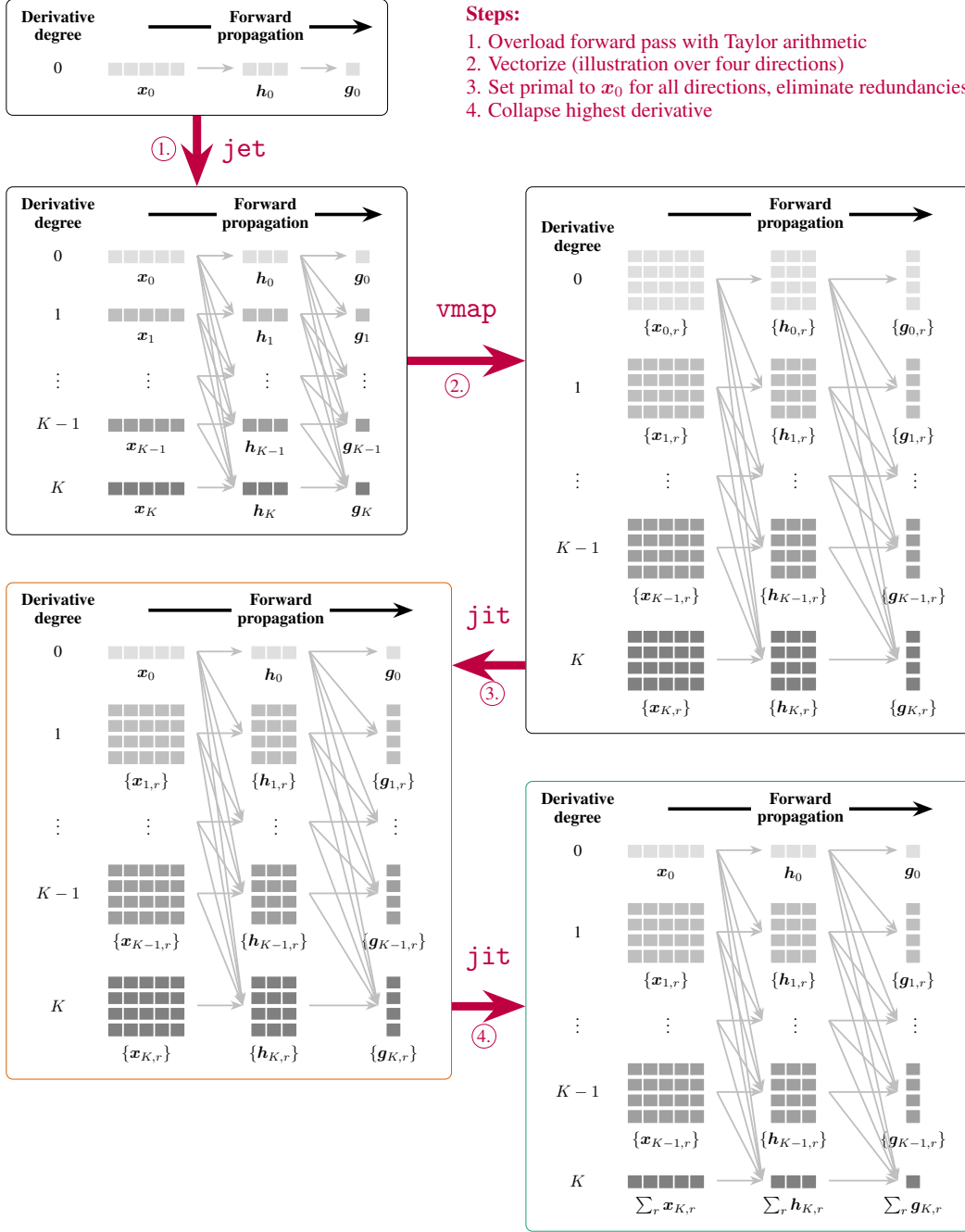


Figure B6: **Step-by-step transformation of a function into its collapsed Taylor mode.** Collapsed Taylor mode can be implemented via the already existing `jet` (standard Taylor mode), `vmap` (vectorization), and `jit` (graph transformation) interfaces. Therefore, users do not need to learn a new interface to benefit from our proposed method and can simply rely on standard Taylor mode and just-in-time compilation (after incorporating our proposed simplifications). Coloured boxes correspond to our PyTorch implementations of `standard` and `collapsed` Taylor mode from our experiments.

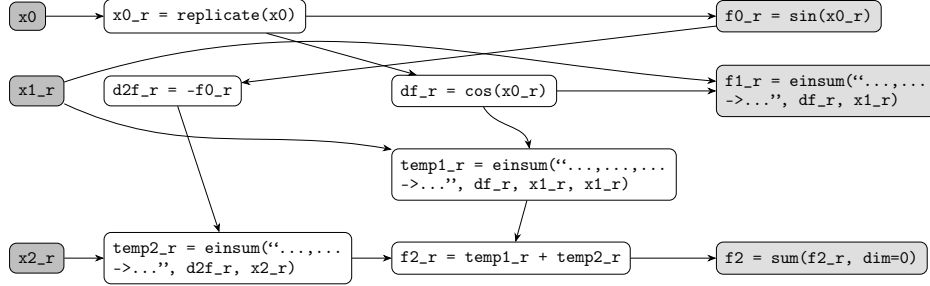
C Graph Simplifications

In this section, we illustrate the two graph simplifications that are required to collapse Taylor mode.

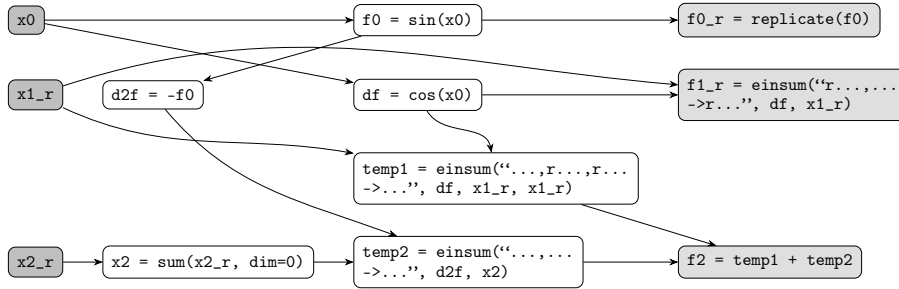
We will consider collapsing the 2-jet of $f = \sin$ as an example. Recall the propagation scheme eq. (D13) and assume that the Taylor coefficients are given by $\{x_{0,r} = x_0\}$, $\{x_{1,r}\}$, and $\{x_{2,r}\}$ where r indexes the directions along which we evaluate the sum:

$$\begin{aligned} & \begin{matrix} x_0 \\ \{x_{1,r}\} \\ \{x_{2,r}\} \end{matrix} \xrightarrow{\text{replicate } x_0} \begin{matrix} x_{0,r} = x_0 \\ x_{1,r} \\ x_{2,r} \end{matrix} \xrightarrow{D13} \begin{matrix} f_{0,r} = \sin(x_0) \\ f_{1,r} = \cos(x_0) \odot x_{1,r} \\ f_{2,r} = -\sin(x_0) \odot x_{1,r} \odot x_{1,r} + \cos(x_0) \odot x_{2,r} \end{matrix} \\ & \xrightarrow{\text{sum highest component}} \begin{matrix} f_{0,r} \\ f_{1,r} \\ \sum_r f_{2,r} \end{matrix} \end{aligned}$$

Here, \sin applies element-wise and \odot denotes element-wise multiplication. The computational graph for this procedure is displayed in the following diagram, with input and output nodes highlighted in dark and light gray. The suffix $_r$ means that all R corresponding tensors are stacked along their leading axis. `replicate` is a function that replicates a tensor R times along a new leading axis, which is in PyTorch usually for free and without additional memory overhead (using `torch.expand`). All other functions refer to those of the PyTorch API:



Our simplification proceeds in two steps. First, propagate `replicate` nodes down the graph to remove repeated computations on the same tensors. This is done in a forward traversal through the graph. Second, in a single backward traversal through the graph, we propagate the sum node up. After applying both steps, the graph looks as follows:



Two important properties of the new graph are (i) the `replicate` node moved to an output node, hence the corresponding redundant computation was successfully removed (ii) the highest component $x_{2,r}$ is immediately summed then propagated, i.e., we collapsed Taylor mode and avoid the separate propagation for all $x_{2,r}$.

We will now illustrate the two simplification steps in full detail. The first stage starts from the original graph and pushes forward the `replicate` node, as illustrated step-by-step in fig. C7. The second stage starts from the graph produced by the `replicate`-push procedure, and propagates the final sum node up the graph, illustrated by fig. C8. This yields the final computation graph shown above.

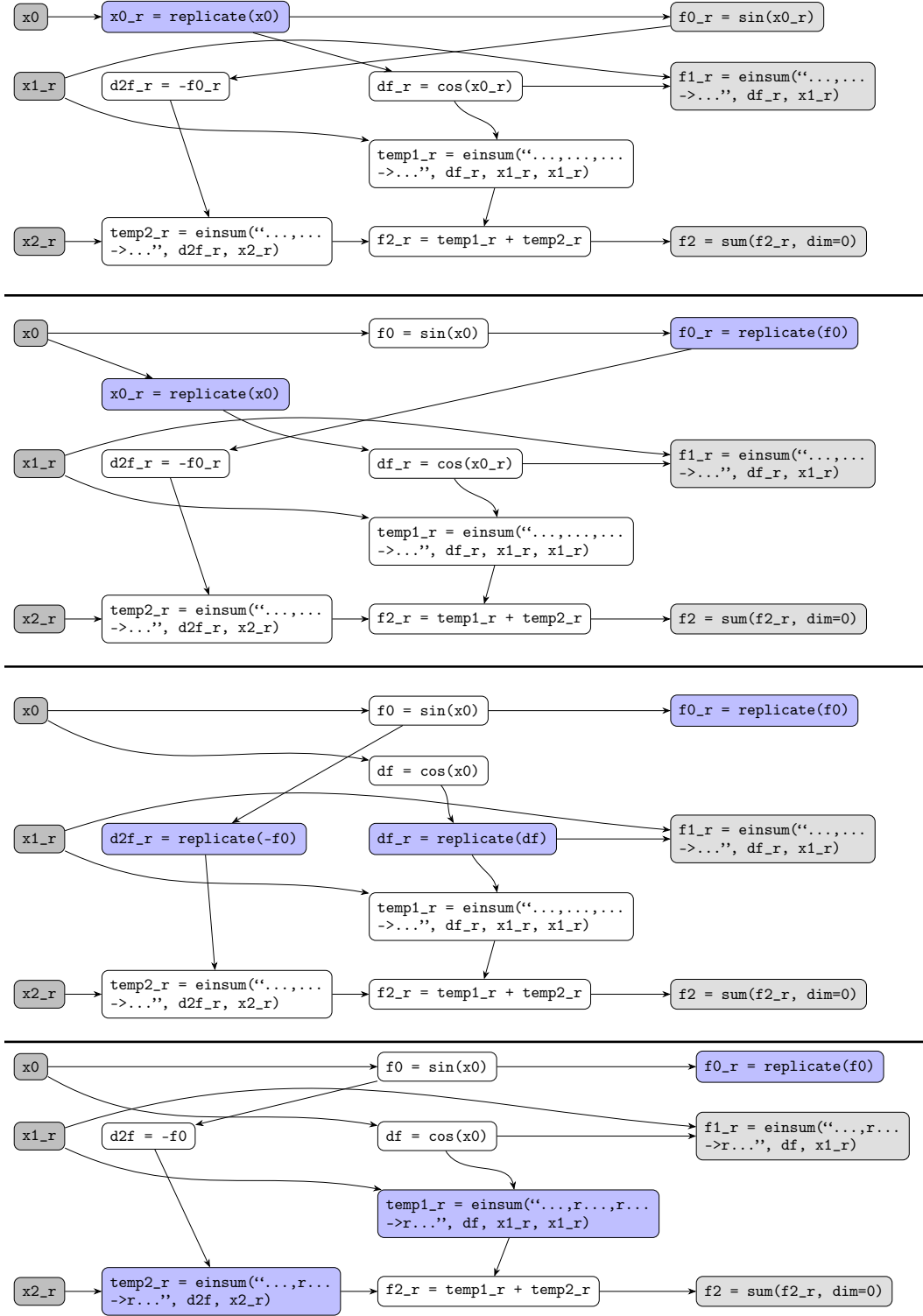


Figure C7: Step-by-step illustration of pushing replicate nodes down a computation graph.

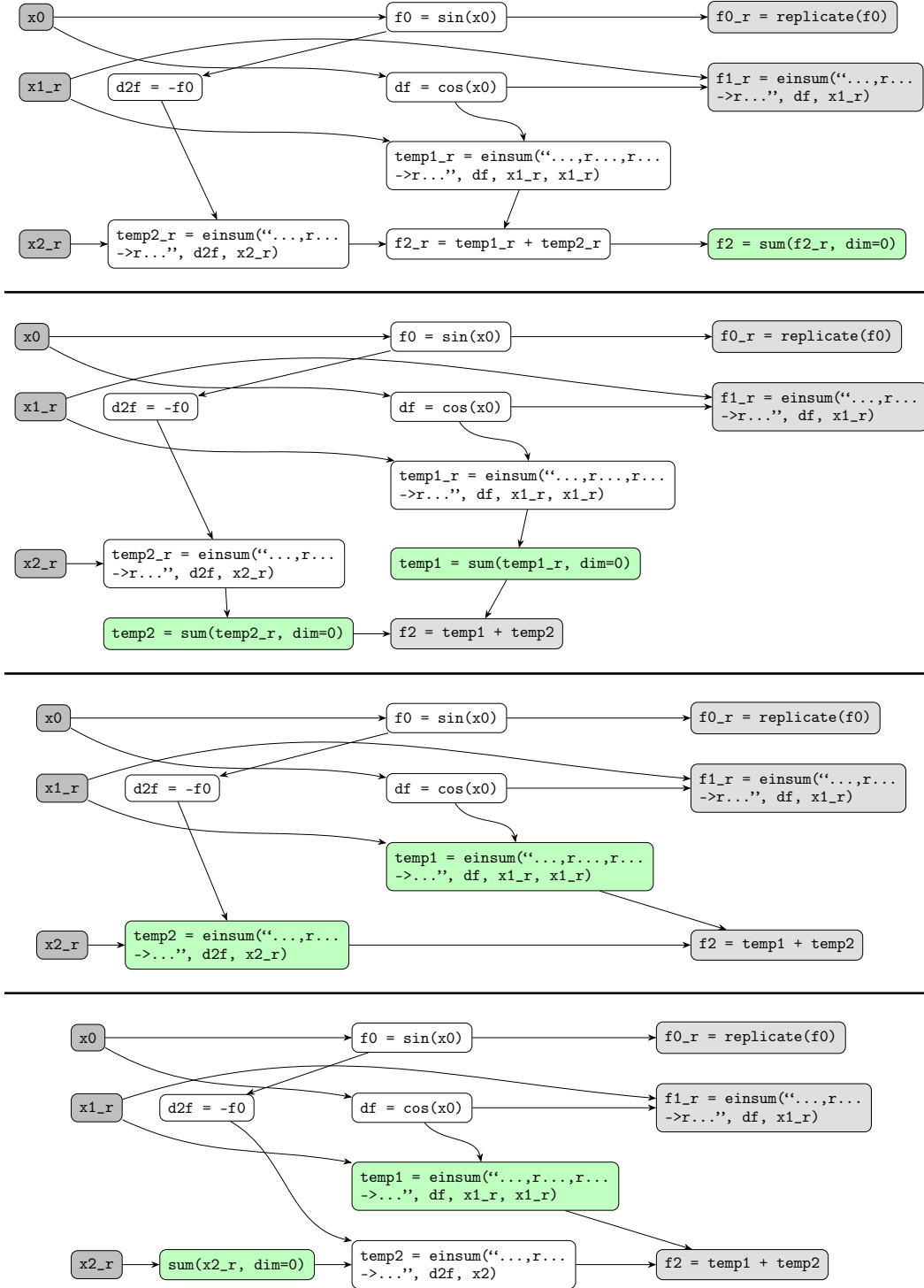


Figure C8: Step-by-step illustration of propagating sum nodes up a computation graph.

D Exploiting Linearity to Collapse Taylor Mode

Here, we present the schematic idea behind propagating R K -jets through $\mathbf{f} = \mathbf{g} \circ \mathbf{h}$ with starting jets $(J^K \mathbf{x})_r(t) = \sum_{k=0}^K \frac{t^k}{k!} \mathbf{x}_{k,r}$. The following Taylor mode AD scheme results from inserting eq. (5) into the eq. (4):

$$\begin{aligned}
 \begin{pmatrix} \mathbf{x}_0 \\ \{\mathbf{x}_{1,r}\} \\ \{\mathbf{x}_{2,r}\} \\ \vdots \\ \{\mathbf{x}_{K,r}\} \end{pmatrix} &\xrightarrow{(3)} \begin{pmatrix} \mathbf{h}_0 = \mathbf{h}(\mathbf{x}_0) \\ \{\mathbf{h}_{1,r}\} = \{\langle \partial \mathbf{h}(\mathbf{x}_0), \mathbf{x}_{1,r} \rangle\} \\ \{\mathbf{h}_{2,r}\} = \{\langle \partial^2 \mathbf{h}(\mathbf{x}_0), \mathbf{x}_{1,r} \otimes \mathbf{x}_{1,r} \rangle + \langle \partial \mathbf{h}(\mathbf{x}_0), \mathbf{x}_{2,r} \rangle\} \\ \vdots \\ \{\mathbf{h}_{K,r}\} = \left\{ \sum_{\sigma \in \text{part}(K)} \nu(\sigma) \left\langle \partial^{|\sigma|} \mathbf{h}(\mathbf{x}_0), \bigotimes_{s \in \sigma} \mathbf{x}_{s,r} \right\rangle \right\} \end{pmatrix} \\
 &\xrightarrow{(3)} \begin{pmatrix} \mathbf{g}_0 = \mathbf{g}(\mathbf{h}_0) \\ \{\mathbf{g}_{1,r}\} = \{\langle \partial \mathbf{g}(\mathbf{h}_0), \mathbf{h}_{1,r} \rangle\} \\ \{\mathbf{g}_{2,r}\} = \{\langle \partial^2 \mathbf{g}(\mathbf{h}_0), \mathbf{h}_{1,r} \otimes \mathbf{h}_{1,r} \rangle + \langle \partial \mathbf{g}(\mathbf{h}_0), \mathbf{h}_{2,r} \rangle\} \\ \vdots \\ \{\mathbf{g}_{K,r}\} = \left\{ \sum_{\sigma \in \text{part}(K)} \nu(\sigma) \left\langle \partial^{|\sigma|} \mathbf{g}(\mathbf{h}_0), \bigotimes_{s \in \sigma} \mathbf{h}_{s,r} \right\rangle \right\} \end{pmatrix} \quad (\text{D13}) \\
 &\stackrel{(3)}{=} \begin{pmatrix} \mathbf{f}_0 = \mathbf{f}(\mathbf{x}_0) \\ \{\mathbf{f}_{1,r}\} = \{\langle \partial \mathbf{f}(\mathbf{x}_0), \mathbf{x}_{1,r} \rangle\} \\ \{\mathbf{f}_{2,r}\} = \{\langle \partial^2 \mathbf{f}(\mathbf{x}_0), \mathbf{x}_{1,r} \otimes \mathbf{x}_{1,r} \rangle + \langle \partial \mathbf{f}(\mathbf{x}_0), \mathbf{x}_{2,r} \rangle\} \\ \vdots \\ \{\mathbf{f}_{K,r}\} = \left\{ \sum_{\sigma \in \text{part}(K)} \nu(\sigma) \left\langle \partial^{|\sigma|} \mathbf{f}(\mathbf{x}_0), \bigotimes_{s \in \sigma} \mathbf{x}_{s,r} \right\rangle \right\} \end{pmatrix} \\
 &\xrightarrow{\text{slice}} \{\mathbf{g}_{K,r}\} \\
 &\xrightarrow{\text{sum}} \sum_{r=1}^R \mathbf{g}_{K,r} \big|_{\{\mathbf{x}_{1,r}=\mathbf{v}_r, \mathbf{x}_{2,r}=\dots=\mathbf{x}_{K,r}=\mathbf{0}\}} \sum_{r=1}^R \langle \partial^K \mathbf{f}(\mathbf{x}_0), \bigotimes_{k=1}^K \mathbf{v}_r \rangle
 \end{aligned}$$

Leveraging linearity in certain terms (in green) of the highest coefficient, as explained in eq. (6), instead leads to

$$\begin{aligned}
 \begin{pmatrix} \mathbf{x}_0 \\ \{\mathbf{x}_{1,r}\} \\ \{\mathbf{x}_{2,r}\} \\ \vdots \\ \sum_{r=1}^R \mathbf{x}_{K,r} \end{pmatrix} &\xrightarrow{(3)} \begin{pmatrix} \mathbf{h}_0 = \mathbf{h}(\mathbf{x}_0) \\ \{\mathbf{h}_{1,r}\} = \{\langle \partial \mathbf{h}(\mathbf{x}_0), \mathbf{x}_{1,r} \rangle\} \\ \{\mathbf{h}_{2,r}\} = \{\langle \partial^2 \mathbf{h}(\mathbf{x}_0), \mathbf{x}_{1,r} \otimes \mathbf{x}_{1,r} \rangle + \langle \partial \mathbf{h}(\mathbf{x}_0), \mathbf{x}_{2,r} \rangle\} \\ \vdots \\ \sum_{r=1}^R \mathbf{h}_{K,r} = \sum_{r=1}^R \sum_{\sigma \in \text{part}(K) \setminus \{\sigma_t\}} \nu(\sigma) \left\langle \partial^{|\sigma|} \mathbf{h}(\mathbf{x}_0), \bigotimes_{s \in \sigma} \mathbf{x}_{s,r} \right\rangle \\ \quad + \left\langle \partial \mathbf{h}(\mathbf{x}_0), \sum_{r=1}^R \mathbf{x}_{K,r} \right\rangle \end{pmatrix} \\
 &\xrightarrow{(3)} \begin{pmatrix} \mathbf{g}_0 = \mathbf{g}(\mathbf{h}_0) \\ \{\mathbf{g}_{1,r}\} = \{\langle \partial \mathbf{g}(\mathbf{h}_0), \mathbf{h}_{1,r} \rangle\} \\ \{\mathbf{g}_{2,r}\} = \{\langle \partial^2 \mathbf{g}(\mathbf{h}_0), \mathbf{h}_{1,r} \otimes \mathbf{h}_{1,r} \rangle + \langle \partial \mathbf{g}(\mathbf{h}_0), \mathbf{h}_{2,r} \rangle\} \\ \vdots \\ \sum_{r=1}^R \mathbf{g}_{K,r} = \sum_{r=1}^R \sum_{\sigma \in \text{part}(K) \setminus \{\sigma_t\}} \nu(\sigma) \left\langle \partial^{|\sigma|} \mathbf{g}(\mathbf{h}_0), \bigotimes_{s \in \sigma} \mathbf{h}_{s,r} \right\rangle \\ \quad + \left\langle \partial \mathbf{g}(\mathbf{h}_0), \sum_{r=1}^R \mathbf{h}_{K,r} \right\rangle \end{pmatrix} \quad (\text{D14})
 \end{aligned}$$

$$\begin{aligned}
& \begin{pmatrix} \mathbf{f}_0 & = \mathbf{f}(\mathbf{x}_0) \\ \{\mathbf{f}_{1,r}\} & = \{\langle \partial \mathbf{f}(\mathbf{x}_0), \mathbf{x}_{1,r} \rangle\} \\ \{\mathbf{f}_{2,r}\} & = \{\langle \partial^2 \mathbf{f}(\mathbf{x}_0), \mathbf{x}_{1,r} \otimes \mathbf{x}_{1,r} \rangle + \langle \partial \mathbf{f}(\mathbf{x}_0), \mathbf{x}_{2,r} \rangle\} \\ \vdots & \\ \sum_{r=1}^R \mathbf{f}_{K,r} & = \sum_{r=1}^R \sum_{\sigma \in \text{part}(K) \setminus \{\sigma_t\}} \nu(\sigma) \left\langle \partial^{|\sigma|} \mathbf{f}(\mathbf{x}_0), \bigotimes_{s \in \sigma} \mathbf{x}_{s,r} \right\rangle \\ & \quad + \left\langle \partial \mathbf{f}(\mathbf{x}_0), \sum_{r=1}^R \mathbf{x}_{K,r} \right\rangle \end{pmatrix} \\
& \xrightarrow{\text{slice}} \sum_{r=1}^R \mathbf{g}_{K,r} \quad \{\mathbf{x}_{1,r} = \mathbf{v}_r, \mathbf{x}_{2,r} = \dots = \mathbf{x}_{K,r} = \mathbf{0}\} \sum_{r=1}^R \langle \partial^K \mathbf{f}(\mathbf{x}_0), \bigotimes_{k=1}^K \mathbf{v}_r \rangle
\end{aligned}$$

D.1 Second-order Operators — Laplacian

Here, we will show details about the propagation schemes of the standard Taylor mode and the collapsed Taylor mode for the computation of the Laplacian of \mathbf{f} . We consider the decomposition $\mathbf{f} = \mathbf{g} \circ \mathbf{h}$.

Standard Taylor Mode AD Using standard Taylor mode (see eq. (D13)) to compute the Laplacian we obtain

$$\begin{aligned}
& \begin{pmatrix} \mathbf{x}_0 \\ \{\mathbf{x}_{1,d}\} \\ \{\mathbf{x}_{2,d}\} \end{pmatrix} \xrightarrow{(3)} \begin{pmatrix} \mathbf{h}_0 = \mathbf{h}(\mathbf{x}_0) \\ \{\mathbf{h}_{1,d}\} = \{\langle \partial \mathbf{h}(\mathbf{x}_0), \mathbf{x}_{1,d} \rangle\} \\ \{\mathbf{h}_{2,d}\} = \{\langle \partial^2 \mathbf{h}(\mathbf{x}_0), \mathbf{x}_{1,d} \otimes \mathbf{x}_{1,d} \rangle + \langle \partial \mathbf{h}(\mathbf{x}_0), \mathbf{x}_{2,d} \rangle\} \end{pmatrix} \\
& \xrightarrow{(3)} \begin{pmatrix} \mathbf{g}_0 = \mathbf{g}(\mathbf{h}_0) \\ \{\mathbf{g}_{1,d}\} = \{\langle \partial \mathbf{g}(\mathbf{h}_0), \mathbf{h}_{1,d} \rangle\} \\ \{\mathbf{g}_{2,d}\} = \{\langle \partial^2 \mathbf{g}(\mathbf{h}_0), \mathbf{h}_{1,d} \otimes \mathbf{h}_{1,d} \rangle + \langle \partial \mathbf{g}(\mathbf{h}_0), \mathbf{h}_{2,d} \rangle\} \end{pmatrix} \\
& \stackrel{(3)}{=} \begin{pmatrix} \mathbf{f}_0 = \mathbf{f}(\mathbf{x}_0) \\ \{\mathbf{f}_{1,d}\} = \{\langle \partial \mathbf{f}(\mathbf{x}_0), \mathbf{x}_{1,d} \rangle\} \\ \{\mathbf{f}_{2,d}\} = \{\langle \partial^2 \mathbf{f}(\mathbf{x}_0), \mathbf{x}_{1,d} \otimes \mathbf{x}_{1,d} \rangle + \langle \partial \mathbf{f}(\mathbf{x}_0), \mathbf{x}_{2,d} \rangle\} \end{pmatrix} \quad (D15) \\
& \xrightarrow{\text{slice}} \{\mathbf{g}_{2,d}\} \\
& \xrightarrow{\text{sum}} \sum_{d=1}^D \{\mathbf{g}_{2,d}\} \quad \{\mathbf{x}_{1,d} = \mathbf{e}_d, \mathbf{x}_{2,d} = \mathbf{0}\} \Delta \mathbf{f}(\mathbf{x}_0).
\end{aligned}$$

Collapsed Taylor Mode AD Using our proposed collapsed Taylor mode, we get

$$\begin{aligned}
& \begin{pmatrix} \mathbf{x}_0 \\ \{\mathbf{x}_{1,d}\} \\ \sum_{d=1}^D \mathbf{x}_{2,d} \end{pmatrix} \xrightarrow{(1)} \begin{pmatrix} \mathbf{h}_0 = \mathbf{h}(\mathbf{x}_0) \\ \{\mathbf{h}_{1,d}\} = \{\langle \partial \mathbf{h}(\mathbf{x}_0), \mathbf{x}_{1,d} \rangle\} \\ \sum_{d=1}^D \mathbf{h}_{2,d} = \sum_{d=1}^D \langle \partial^2 \mathbf{h}(\mathbf{x}_0), \mathbf{x}_{1,d} \otimes \mathbf{x}_{1,d} \rangle + \left\langle \partial \mathbf{h}(\mathbf{x}_0), \sum_{d=1}^D \mathbf{x}_{2,d} \right\rangle \end{pmatrix} \\
& \xrightarrow{(1)} \begin{pmatrix} \mathbf{g}_0 = \mathbf{g}(\mathbf{h}_0) \\ \{\mathbf{g}_{1,d}\} = \{\langle \partial \mathbf{g}(\mathbf{h}_0), \mathbf{h}_{1,d} \rangle\} \\ \sum_{d=1}^D \mathbf{g}_{2,d} = \sum_{d=1}^D \langle \partial^2 \mathbf{g}(\mathbf{h}_0), \mathbf{h}_{1,d} \otimes \mathbf{h}_{1,d} \rangle + \left\langle \partial \mathbf{g}(\mathbf{h}_0), \sum_{d=1}^D \mathbf{h}_{2,d} \right\rangle \end{pmatrix} \quad (D16) \\
& \stackrel{(1)}{=} \begin{pmatrix} \mathbf{f}_0 = \mathbf{f}(\mathbf{x}_0) \\ \{\mathbf{f}_{1,d}\} = \{\langle \partial \mathbf{f}(\mathbf{x}_0), \mathbf{x}_{1,d} \rangle\} \\ \sum_{d=1}^D \mathbf{f}_{2,d} = \sum_{d=1}^D \langle \partial^2 \mathbf{f}(\mathbf{x}_0), \mathbf{x}_{1,d} \otimes \mathbf{x}_{1,d} \rangle + \left\langle \partial \mathbf{f}(\mathbf{x}_0), \sum_{i=1}^D \mathbf{x}_{2,i} \right\rangle \end{pmatrix} \\
& \xrightarrow{\text{slice}} \sum_{d=1}^D \{\mathbf{g}_{2,d}\} \quad \{(\mathbf{x}_{1,d} = \mathbf{e}_d, \mathbf{x}_{2,d} = \mathbf{0})\} \Delta \mathbf{f}(\mathbf{x}_0)
\end{aligned}$$

E Details on (Collapsed) Taylor Mode for Arbitrary Mixed Partial Derivatives

This section introduces the notation we used in eq. (11). The right side of the formula sums over all $\mathbf{j} \in \mathbb{N}^I$ such that $\|\mathbf{j}\|_1 := \sum_i [\mathbf{j}]_i = K$. If $I = 2$ and $\|\mathbf{j}\|_1 = 4$, this index-set consists of $\{(4, 0), (0, 4), (3, 1), (1, 3), (2, 2)\}$.

The coefficient $\gamma_{\mathbf{i}, \mathbf{j}}$ is defined as

$$\gamma_{\mathbf{i}, \mathbf{j}} := \sum_{0 < \mathbf{m} \leq \mathbf{i}} (-1)^{\|\mathbf{i} - \mathbf{m}\|_1} \binom{\mathbf{i}}{\mathbf{m}} \binom{\|\mathbf{i}\|_1 \frac{\mathbf{m}}{\|\mathbf{m}\|_1}}{\mathbf{j}} \left(\frac{\|\mathbf{m}\|_1}{\|\mathbf{i}\|_1} \right)^{\|\mathbf{i}\|_1}. \quad (\text{E17})$$

The summation ranges over the set $\{\mathbf{m} \in \mathbb{N}^I \mid [\mathbf{m}]_1 \leq [\mathbf{i}]_1, \dots, [\mathbf{m}]_I \leq [\mathbf{i}]_I, \|\mathbf{m}\|_1 > 0\}$. Furthermore, we utilize the generalized binomial coefficient

$$\binom{a}{b} := \prod_{l=0}^{b-1} \frac{a-l}{b-l} \quad (\text{E18})$$

to allow the computation for all $a \in \mathbb{R}$ and $b \in \mathbb{N}$, which is defined to be 1 if $b = 0$. The generalized binomial coefficient of vectors is the product of all generalized binomial coefficients of the components: $\binom{\mathbf{a}}{\mathbf{b}} := \prod_{i=1}^I \binom{[\mathbf{a}]_i}{[\mathbf{b}]_i}$. This notation also includes cases where the vector has components of \mathbb{R} .

E.1 Applied to the Biharmonic Operator

To compute eq. (9) with eq. (11), we first select $K = 4, I = 2, D_1 = D_2 = D, \mathbf{i} = (2, 2), \mathbf{v}_{d_1} = \mathbf{e}_{d_1}$ and $\mathbf{e}_{d_2} = \mathbf{e}_{d_2}$. Then we insert these parameters into the general equation eq. (11) and get

$$\begin{aligned} \Delta^2 \mathbf{f}(\mathbf{x}_0) &= \sum_{\mathbf{j} \in \mathbb{N}^2, \|\mathbf{j}\|_1=4} \gamma_{(2,2), \mathbf{j}} \frac{1}{4!} \sum_{d_1=1}^D \sum_{d_2=1}^D \left\langle \partial^4 \mathbf{f}(\mathbf{x}_0), (\mathbf{e}_{d_1}[\mathbf{j}]_1 + \mathbf{e}_{d_2}[\mathbf{j}]_2)^{\otimes 4} \right\rangle \\ &= \frac{1}{24} \left(\gamma_{(2,2), (4,0)} \sum_{d_1=1}^D \sum_{d_2=1}^D \left\langle \partial^4 \mathbf{f}(\mathbf{x}_0), (4\mathbf{e}_{d_1})^{\otimes 4} \right\rangle \right. \\ &\quad + \gamma_{(2,2), (0,4)} \sum_{d_1=1}^D \sum_{d_2=1}^D \left\langle \partial^4 \mathbf{f}(\mathbf{x}_0), (4\mathbf{e}_{d_2})^{\otimes 4} \right\rangle \\ &\quad + \gamma_{(2,2), (3,1)} \sum_{d_1=1}^D \sum_{d_2=1}^D \left\langle \partial^4 \mathbf{f}(\mathbf{x}_0), (3\mathbf{e}_{d_1} + \mathbf{e}_{d_2})^{\otimes 4} \right\rangle \\ &\quad + \gamma_{(2,2), (1,3)} \sum_{d_1=1}^D \sum_{d_2=1}^D \left\langle \partial^4 \mathbf{f}(\mathbf{x}_0), (\mathbf{e}_{d_1} + 3\mathbf{e}_{d_2})^{\otimes 4} \right\rangle \\ &\quad \left. + \gamma_{(2,2), (2,2)} \sum_{d_1=1}^D \sum_{d_2=1}^D \left\langle \partial^4 \mathbf{f}(\mathbf{x}_0), (2\mathbf{e}_{d_1} + 2\mathbf{e}_{d_2})^{\otimes 4} \right\rangle \right). \end{aligned} \quad (\text{E19})$$

Afterwards, we exploit the symmetry of the coefficients $\gamma_{(2,2), (4,0)} = \gamma_{(2,2), (0,4)}$ and $\gamma_{(2,2), (3,1)} = \gamma_{(2,2), (1,3)}$ yielding

$$\begin{aligned}
& \frac{1}{24} \left(2D\gamma_{(2,2),(4,0)} \sum_{d_1=1}^D \left\langle \partial^4 \mathbf{f}(\mathbf{x}_0), (4\mathbf{e}_{d_1})^{\otimes 4} \right\rangle \right. \\
& + 2\gamma_{(2,2),(3,1)} \sum_{d_1=1}^D \sum_{d_2=1}^D \left\langle \partial^4 \mathbf{f}(\mathbf{x}_0), (3\mathbf{e}_{d_1} + \mathbf{e}_{d_2})^{\otimes 4} \right\rangle \\
& \left. + \gamma_{(2,2),(2,2)} \sum_{d_1=1}^D \sum_{d_2=1}^D \left\langle \partial^4 \mathbf{f}(\mathbf{x}_0), (2\mathbf{e}_{d_1} + 2\mathbf{e}_{d_2})^{\otimes 4} \right\rangle \right). \tag{E20}
\end{aligned}$$

Since the first sum captures all diagonal directions $e_{d_1} = e_{d_2}$, we extract this from the second and third sums to further reduce the computational effort. We obtain

$$\begin{aligned}
& \frac{1}{24} \left((2D\gamma_{(2,2),(4,0)} + 2\gamma_{(2,2),(3,1)} + \gamma_{(2,2),(2,2)}) \sum_{d_1=1}^D \left\langle \partial^4 \mathbf{f}(\mathbf{x}_0), (4\mathbf{e}_{d_1})^{\otimes 4} \right\rangle \right. \\
& + 2\gamma_{(2,2),(3,1)} \sum_{d_1=1}^D \sum_{\substack{d_2=1 \\ d_2 \neq d_1}}^D \left\langle \partial^4 \mathbf{f}(\mathbf{x}_0), (3\mathbf{e}_{d_1} + \mathbf{e}_{d_2})^{\otimes 4} \right\rangle \\
& \left. + \gamma_{(2,2),(2,2)} \sum_{d_1=1}^D \sum_{\substack{d_2=1 \\ d_2 \neq d_1}}^D \left\langle \partial^4 \mathbf{f}(\mathbf{x}_0), (2\mathbf{e}_{d_1} + 2\mathbf{e}_{d_2})^{\otimes 4} \right\rangle \right). \tag{E21}
\end{aligned}$$

Exploiting further symmetries, one obtains

$$\begin{aligned}
\Delta^2 \mathbf{f}(\mathbf{x}_0) &= \frac{1}{24} \left((2D\gamma_{(2,2),(4,0)} + 2\gamma_{(2,2),(3,1)} + \gamma_{(2,2),(2,2)}) \sum_{d_1=1}^D \left\langle \partial^4 \mathbf{f}(\mathbf{x}_0), (4\mathbf{e}_{d_1})^{\otimes 4} \right\rangle \right. \\
& + 2\gamma_{(2,2),(3,1)} \sum_{d_1=1}^D \sum_{\substack{d_2=1 \\ d_2 \neq d_1}}^D \left\langle \partial^4 \mathbf{f}(\mathbf{x}_0), (3\mathbf{e}_{d_1} + \mathbf{e}_{d_2})^{\otimes 4} \right\rangle \\
& \left. + 2\gamma_{(2,2),(2,2)} \sum_{d_1=1}^{D-1} \sum_{d_2=d_1+1}^D \left\langle \partial^4 \mathbf{f}(\mathbf{x}_0), (2\mathbf{e}_{d_1} + 2\mathbf{e}_{d_2})^{\otimes 4} \right\rangle \right). \tag{E22}
\end{aligned}$$

E.2 Pedagogical Approach for the Biharmonic Operator with 6-jets

A different approach to compute arbitrary-mixed derivatives was proposed in [26]. This approach relies, for the biharmonic operator, on the hand-selection of certain 6-jets to extract the required derivatives. The degree and directions for the jets are obtained by considering the Faà di Bruno formula for the 6-th coefficient \mathbf{f}_6 (see §A). Selecting coefficients of the input 6-jet to $\mathbf{x}_1 = \mathbf{e}_{d_1}$, $\mathbf{x}_2 = \mathbf{e}_{d_2}$ and $\mathbf{x}_3 = \mathbf{x}_4 = \mathbf{x}_5 = \mathbf{x}_6 = \mathbf{0}$ leads us to

$$\begin{aligned}
\mathbf{f}_6 &= \langle \partial^6 \mathbf{f}(\mathbf{x}_0), \otimes_{k=1}^6 \mathbf{e}_{d_1} \rangle + 15 \left\langle \partial^5 \mathbf{f}(\mathbf{x}_0), (\mathbf{e}_{d_1})^{\otimes 4} \otimes \mathbf{e}_{d_2} \right\rangle \\
& + 45 \left\langle \partial^4 \mathbf{f}(\mathbf{x}_0), (\mathbf{e}_{d_1})^{\otimes 2} \otimes (\mathbf{e}_{d_2})^{\otimes 2} \right\rangle + 15 \left\langle \partial^3 \mathbf{f}(\mathbf{x}_0), \otimes_{k=1}^3 \mathbf{e}_{d_2} \right\rangle. \tag{E23}
\end{aligned}$$

Notice the **blue term**, which has the same structure as the summands we want to compute for the biharmonic operator. Therefore, a first 6-jet is computed as explained above. To cancel out the unwanted terms, we evaluate another 6-jet with the same input except $\mathbf{x}_2 = -\mathbf{e}_{d_2}$ and adding the 6-th coefficient of this jet to eq. (E23) gives

$$2 \left\langle \partial^6 \mathbf{f}(\mathbf{x}_0), \otimes_{k=1}^6 \mathbf{e}_{d_1} \right\rangle + 90 \left\langle \partial^4 \mathbf{f}(\mathbf{x}_0), (\mathbf{e}_{d_1})^{\otimes 2} \otimes (\mathbf{e}_{d_2})^{\otimes 2} \right\rangle. \tag{E24}$$

Finally, a third 6-jet is computing with $\mathbf{x}_2 = \mathbf{0}$. The 6-th coefficient of this jet contains only

$$\left\langle \partial^6 \mathbf{f}(\mathbf{x}_0), \otimes_{k=1}^6 \mathbf{x}_1 \right\rangle. \tag{E25}$$

We obtain

$$90 \left\langle \partial^4 \mathbf{f}(\mathbf{x}_0), (\mathbf{x}_1)^{\otimes 2} \otimes (\mathbf{x}_2)^{\otimes 2} \right\rangle \quad (\text{E26})$$

by subtracting twice of the 6-th coefficient of the third jet from eq. (E24).

To summarize the procedure, we evaluate the 6-jet three times. The first jet has the input $\mathbf{x}_1 = \mathbf{e}_{d_1}$, $\mathbf{x}_2 = \mathbf{e}_{d_2}$ and $\mathbf{x}_3 = \mathbf{x}_4 = \mathbf{x}_5 = \mathbf{x}_6 = \mathbf{0}$, the second jet has the same input jet apart from $\mathbf{x}_2 = \mathbf{e}_{d_2}$. The third 6-jet takes $\mathbf{x}_2 = \mathbf{0}$. Then we add the 6-th coefficient of the first and the second and subtract twice of the 6-th coefficient of the third jet. Dividing by 90 provides the derivative corresponding to the d_1, d_2 term of the biharmonic operator.

The standard Taylor mode would propagate $1 + 18D^2$ vectors through every node, where we already exploit that all jets share \mathbf{x}_0 . Leveraging our collapsed Taylor mode would have the cost of passing $1 + 3 + 15D^2$ vectors to every node of the compute graph. Still, this is very expensive in comparison to our approach described before. In addition, until now, the selection of the jet degree and the input coefficients requires substantial human effort.

F PyTorch Benchmark

Here, we compare the theoretically estimated performance improvements based on counting the number of forward-propagated vectors with the empirically measured performance.

To estimate the performance ratio between standard and collapsed Taylor mode, we can use the number of additional vectors both modes propagate forward as we increase either the batch size or the number of Monte-Carlo samples. This is a relatively simplistic proxy; e.g., it assumes that each vector adds the same computational load, which is inaccurate as vectors corresponding to higher coefficients require more work and memory (as the Faà di Bruno formula contains more terms in general). Conversely, while incrementing the MC samples does add additional vectors that are propagated, it does not introduce additional cost to compute or store the derivatives, as they are already computed with just a single sample. Table F2 summarizes the theoretical and empirical ratios. We find them to align quite well, despite the overly simplistic assumptions.

As concrete example, consider the exact Laplacian. Adding one datum introduces $2 + D$ versus $1 + 2D$ new vectors. For $D = 50$, their ratio is $(2+D)/(1+2D) \approx 0.51$. Empirically, we measure that adding one datum adds **0.60 ms** to standard and **0.33 ms** to collapsed Taylor mode (table 1), whose ratio of ≈ 0.55 is close to the theoretical value.

Table F2: **Comparison of theoretical and empirical performance ratios between standard and collapsed Taylor mode.** We list the number of additional vectors that are used when adding another data point (exact) or another Monte-Carlo sample (stochastic). The ratio of vectors offers a good estimate of the empirically measured performance ratio.

Mode	Add one datum or MC sample	Laplacian ($D = 50$)	Weighted Laplacian ($D = R = 50$)	Biharmonic ($D = 5$)
Exact	Δ vectors (standard)	$1 + 2D$	$1 + 2R$	$6D^2 - 2D + 1$
	Δ vectors (collapsed)	$2 + D$	$2 + R$	$9/2 D^2 - 3/2 D + 4$
	Theoretical ratio Δ/Δ	0.51	0.51	0.77
	Empirical time ratio	0.55	0.55	0.88
	Empirical mem. ratio	0.65	0.65	0.78
Stochastic	Δ vectors (standard)	2	2	4
	Δ vectors (collapsed)	1	1	3
	Theoretical ratio Δ/Δ	0.5	0.5	0.75
	Empirical time ratio	0.54	0.54	0.76
	Empirical mem. ratio	0.64	0.64	0.72

G JAX Benchmark

This section presents experiments, which show that the graph simplifications we propose to collapse standard Taylor mode are currently not applied by the `jit` compiler in JAX.

Comparing JAX implementations. Similar to our PyTorch experiment in §4, we compare three implementations of the Laplacian in JAX (all compiled with `jax.jit`):

1. **Nested 1st-order AD** computes the Hessian using `jax.hessian`, which relies on forward-over-reverse mode, then traces it.
2. **Standard Taylor mode** propagates multiple univariate Taylor polynomials, each of which computes one element of the Hessian diagonal, then sums them to obtain the Laplacian. This is implemented with `jax.experimental.jet.jet` and `jax.vmap`.
3. **Collapsed Taylor mode** relies on the forward Laplacian implementation in JAX provided by the `folx` library [12] and implements our proposed collapsed Taylor mode for the specific case of the Laplacian. `folx` also enables leveraging sparsity in the tensors, which is

Table G3: **JAX Benchmark from fig. G9 in numbers.** We fit linear functions and report their slopes, i.e. how much runtime and memory increase when incrementing the batch size. All numbers are shown with two significant digits and bold values are best according to parenthesized values.

Mode	Per-datum cost	Implementation	Laplacian	Biharmonic
Exact	Time [ms]	Nested 1 st -order	0.57 (1.0x)	0.87 (1.0x)
		Standard Taylor	0.84 (1.5x)	1.5 (1.7x)
		Collapsed (ours)	0.29 (0.50x)	0.29 (0.33x)
	Mem. [MiB] (differentiable)	Nested 1 st -order	6.0 (1.0x)	6.8 (1.0x)
		Standard Taylor	5.4 (0.91x)	21 (3.1x)
		Collapsed (ours)	1.7 (0.29x)	2.0 (0.29x)
	Mem. [MiB] (non-diff.)	Nested 1 st -order	1.4 (1.0x)	2.7 (1.0x)
		Standard Taylor	1.7 (1.2x)	2.2 (0.84x)
		Collapsed (ours)	1.4 (0.99x)	1.0 (0.39x)

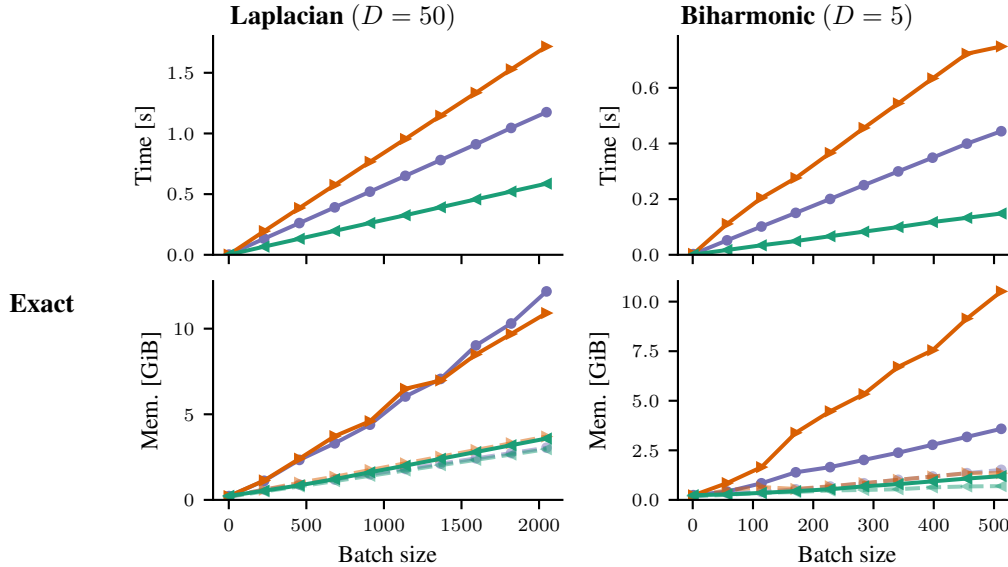


Figure G9: **JAX’s jit compiler does not apply our graph simplifications to standard Taylor mode.** Colors: **Collapsed Taylor mode**, **standard Taylor mode**, and **nested first-order automatic differentiation**, opaque memory consumptions are for non-differentiable computations. Results are on GPU and we use a $D \rightarrow 768 \rightarrow 768 \rightarrow 512 \rightarrow 512 \rightarrow 1$ MLP with tanh activations, varying the batch size. For each approach, we fit a line to the data and report the slope in table G3 to quantify the relative speedup and memory reduction.

beneficial for architectures in VMC. To disentangle runtime improvements from sparsity detection versus collapsing Taylor coefficient, we disable `folx`'s sparsity detection.

For the biharmonic operator, we simply nest the Laplacian implementations.

We only investigate computing the exact Laplacian, as the forward Laplacian in `folx` currently does not support stochastic computation. We use the same neural network architecture as for our PyTorch experiments, fix the input dimension to $D = 50$ and vary the batch size, recording the runtime and peak memory with the same protocol as described in the main text. JAX is purely functional and therefore does not have a mechanism to build up a differentiable computational graph similar to evaluating a function in PyTorch where some leafs have `requires_grad=True`. To approximate the peak memory of computing a differentiable Laplacian in JAX, we measure the peak memory of first computing the Laplacian, then evaluating the gradient w.r.t. the neural network's parameters which backpropagates through the same computation graph built by PyTorch.

Results (Laplacian). The left column of fig. G9 visualizes the performance of the three implementations. We fit linear functions to each of them and report the cost incurred by adding one more datum to the batch in table G3. From them, we draw the following conclusions:

1. **Performance is consistent between PyTorch and JAX.** Although our PyTorch implementation does not leverage compilation, the values reported in tables 1 and G3 are consistent and differ by at most a factor of two (in rare cases). This confirms that our PyTorch-based implementation of Taylor mode is reasonably efficient, and that the presented performance results in the main text are transferable to other frameworks like JAX.
2. **Our implementation of collapsed Taylor mode based on graph rewrites in PyTorch achieves consistent speed-up with the Laplacian-specific implementation in JAX.** Specifically, we observe that `collapsed Taylor mode/forward Laplacian` use roughly half the runtime of `nested 1st-order AD` (compare tables 1 and G3). This supports our argument that our collapsed Taylor is indeed a generalization of the forward Laplacian, i.e., the latter does not employ additional tricks (leveraging sparsity could also be applied to our approach but we are not aware of a drop-in implementation). It also illustrates that the savings we report in PyTorch carry over to other frameworks like JAX.
3. **JAX's jit compiler is unable to apply the graph rewrites we propose in this work.** If the JAX compiler was able to perform our proposed graph rewrites, then the jit-compiled `standard Taylor mode` should yield similar performance than the `forward Laplacian`. However, we observe a clear performance gap in runtime and memory, from which we conclude that the compilation did not collapse the Taylor coefficients. Our contribution is to point out that such rewrites could easily be added to the compiler's ability to unlock these performance gains at zero user overhead.

Results (biharmonic operator). For the biharmonic operator (right column of fig. G9 and table G3), we conclude that (i) the most efficient way to compute biharmonics is by nesting Laplacians (compare with table 1 where Taylor mode uses the approach for general linear differential operators) and (ii) that nesting Taylor mode Laplacians is more efficient than nesting 1st-order AD Laplacians, while also allowing to apply our collapsing technique.